CHARLES UNIVERSITY IN PRAGUE, FACULTY OF SCIENCE

Institute of Hydrogeology, Engineering Geology, and Applied Geophysics

Thermal relations leading to the formation of gaseous phase within the ice covering lakes and ponds

Teplotní vztahy vedoucí ke vzniku plynné fáze v ledu rybníků a jezer

MASTER THESIS

Diplomová práce

Bc. Jolana Hrubá

Supervisor / Vedoucí práce: RNDr. Günther Kletetschka, Ph.D.

Prague 2013

Statement of authorship:

I declare that I am author of this thesis and that I have cited all resources used in its preparation. Neither this thesis nor its substantial part has been submitted to fulfill requirements for other master or any other academic degree.

Prohlášení:

Prohlašuji, že jsem závěrečnou práci zpracovala samostatně a že jsem uvedla všechny použité informační zdroje a literaturu. Tato práce ani její podstatná část nebyla předložena k získání jiného nebo stejného akademického titulu.

In Prague, August 21, 2013

Signature

ACKNOWLEDGEMENT

I would like to acknowledge a gratitude to my supervisor, RNDr. Günther Kleteschka, Ph.D., for his help, valuable suggestions and comments that made this thesis possible.

For his support and patience, I would like to thank Marek Hora. I thank him and many others for the help with the field work.

Many thanks also belong to my family and friends for supporting me during writing of this thesis as well as at every other important moment during my studies.

SUMMARY

When cutting an ice from lakes and ponds gaseous phase displays often ubiquitous bubble textures along the ice thickness. The occurrence of bubbles (enclosures filled with the gas) in ice relates to a content of the dissolved gas in the lake/pond water prior to freezing over the surface. When water freezes, dissolved gases are rejected and redistributed at the ice-water interface, depending on the saturation ratio between the gas and water. If the concentration of dissolved gases surpasses a critical value (as freezing progresses), the water at the interface becomes supersaturated, and gas bubbles nucleate and grow to a visible size along the interface. The bubbles generated at the ice-water interface are either incorporated into the ice crystal as the ice-water interface advances, thus forming gas pores in the ice, or released from the interface. If there is incorporation or release is determined by several factors. The bubbles nucleated at the advancing ice-water interface may be characterized by concentration, shape, and size, which depend on growth rate of ice, the amount of gases dissolved in water, and the particulate content of water.

This work focused on the relation between growth rates of the ice and the occurrence of bubbles in the pond ice. I monitored the temperature of the ice formed under natural conditions over the pond Dolní Tušimy in Mokrovraty, Czech Republic.

Distinct layers of gas bubbles were observed when the ice samples have been retrieved. These layers may relate to fast growth rates of ice. In this case the maximum growth rates were about 1 μm/s.

The results were compared with similar work done (Carte, 1961; Bari and Hallet, 1974; Yoshimura et al., 2008). This comparison showed distinction that may be due to different methods of ice formation (laboratory condition vs. natural conditions).

ABSTRAKT

Jak led na rybnících a jezerech roste, objevuje se v něm často plynná fáze v podobě malých bublin (plynných inkluzí). Jejich výskyt v ledu souvisí s obsahem rozpuštěných plynů ve vodě, ze které led vzniká. Jak se voda postupně mění v led, rozpuštěné plyny jsou v závislosti na poměru nasycení mezi plynem a vodou zachyceny a uspořádány na rozhraní voda-led. Jestliže zde jejich koncentrace dosáhne kritické hodnoty, voda na rozhraní se stává nasycenou a dochází ke tvorbě bublinek. Ty postupně rostou až do pouhým okem viditelné velikosti.

Bubliny, vytvořené na rozhraní voda-led, mohou být začleněny do krystalu ledu, a tak se podílet na jeho pórovitosti, nebo mohou být uvolněny zpět do vody. To, ke kterému procesu dojde, je ovlivněno mnoha faktory. Plynné bubliny v ledu mohou být charakterizovány koncentrací, tvarem a velikostí. Tyto vlastnosti závisí na rychlosti růstu daného ledu, množství rozpuštěných plynů ve vodě a obsahu pevných částic ve vodě, které mohou sloužit jako nukleační centra.

Tato práce je zaměřena na vztah mezi výskytem bublin v ledu a rychlostí jeho růstu. Pro studii byl použit led vytvořený přirozenou cestou na rybníku Dolní Tušimy v Mokrovratech.

Ve vzorcích ledu byly pozorovány zřetelné vrstvy bublin přisuzované vysokým rychlostem růstu ledu. Ty v tomto případě byly okolo 1 μm/s.

Výsledky byly porovnány s již existujícími pracemi na toto téma. Především pak s experimenty Carteho (1961), Bariho a Halletta (1974) a Yoshimury a kol. (2008). Tato porovnání ukázala určité rozdíly, které byly pravděpodobně způsobeny odlišnými metodami, které byly použity pro tvorbu ledu (laboratorní podmínky versus přirozené podmínky).

TABLE OF CONTENTS

LIST OF FIGURES

LIST OF TABLES

1. INTRODUCTION

Ice over lakes and ponds often contain small gas bubbles enclosed in it. These bubbles are generated at the ice-water interface, as freezing progresses, and their occurrence in ice relates to the content of the dissolved gas in water of the lake or pond before it changes into ice. The bubbles vary in size, concentration and shape, and their features depend on such factors as the amount of gases dissolved in water, the particulate content of the water, and growth rates of ice.

This work is focused on the relation between growth rates of ice and the occurrence of bubbles in ice. Previous studies showed that the ice growth rate affect the size, shape, concentration and distribution of bubbles. The main purpose of this work was to investigate the dependence of bubbles in ice on growth rates of the ice and compare the results with the literature.

For the study was used the ice formed under natural condition over the pond Dolní Tušimy in Mokrovraty, Czech Republic. The temperature of the water of the pond and the temperature of the ice were monitored by temperature loggers iButtons. Temperature record was then used for the determination of growth rates of ice. The ice structure was investigated from ice samples retrieved. For the comparison temperature records and ice samples from one other pond were used.

First part of the work dedicates to the structure and classification of lake/pond ice cover, formation of gas bubbles in ice, their shape and gas content. Some methods for predicting the thickness of ice are listed. The second part is focused on the study on the pond Dolní Tušimy itself. It describes the field area, used methods and materials, obtained results and their discussion.

This work deal with bubbles formed at the ice-water interface but also mentions others types of bubbles which may occur in ice. The main goal of the work was to reveal the relation between growth rates of ice and the occurrence of bubbles in ice, but it shows a possible utilization of iButtons data loggers as well.

1.1 Structure and classification of lake and pond ice cover

Lake and pond ice cover is mostly seasonal and occurs where average daily temperature drops below the freezing point (0° C) (Prowse et al., 2007; Rafferty 2012). Lakes and ponds at high latitudes or high altitudes are ice-covered part of the year; typically from November to April and in the very north sometimes from October to early June. Arctic lakes may be ice covered throughout the year and at mid latitudes occasional ice cover may appear for short periods several times during the winter (Bengtsson, 2012a). The formation of ice cover and its disappearance depends on climate factors such as air temperature, cloud cover, and wind. Conditions such as heavy rains or snowmelt in locations upstream or elsewhere in the watershed also affect ice cover duration (Livingstone et al., 2010).

As the air above the water surface cools, the water at the top of lake/pond loses heat, becomes denser than the water below and sinks. This process continues until all the water in the lake/pond is at 4 °C, when the density of water is at its maximum. With further cooling (and without mechanical mixing) a stable, lighter layer of water forms at the surface. As this layer cools to its freezing point, ice begins to form (Ashton, 1986).

Ice on lakes and ponds grows in a static way; there is no horizontal transfer of ice and the ice grows in the vertical direction once the initial ice covers the lake (Bengtsson, 2012b). Ice crystals grow downward into the water column by a congelation process that produces congelation ice (Ashton, 1986).

Congelation ice forms as water freezes at the bottom of ice cover and the latent heat of crystallization is conducted upwards through the ice to the atmosphere. Its growth rate is proportional to the rate at which energy is transferred from the bottom surface of the ice layer to the air above (Bengtsson, 2012b; Jeffries and Morris, 2006; Rafferty, 2012). Congelation ice forms as two major types. The first type is formed by spontaneous nucleation which takes place on cold calm nights when the surface of the lake/pond supercools (the temperature drops below freezing) and the ice nucleates – spreading rapidly across the lake/pond ice surface. Under ideal conditions the first crystals of ice can reach meter wide dimensions. The second type occurs, when lake/pond conditions are cold enough and it is exposed to strong winds blowing dust, snow or frozen rain on the lake/pond surface. It causes heterogeneous nucleation of small ice crystals (nucleation begins at the surface of foreign particles) (Rafferty, 2012).

The congelation ice is usually overlain by snow ice. It forms in several ways. Snow deposited on a thin ice cover can depress the ice surface below the waterline, allowing the water to flow up through cracks and holes to the ice surface. Saturated snow then freezes. Rain and melting snow can percolate downward and refreeze in the lower levels of an unconsolidated snow pack (Ashton, 1986; Leppäranta and Kosloff, 2000; Jeffries and Morris, 2006). The frozen

snow ice has much smaller crystals and is easily recognized from the underlying congelation ice (Gow and Langston, 1977).

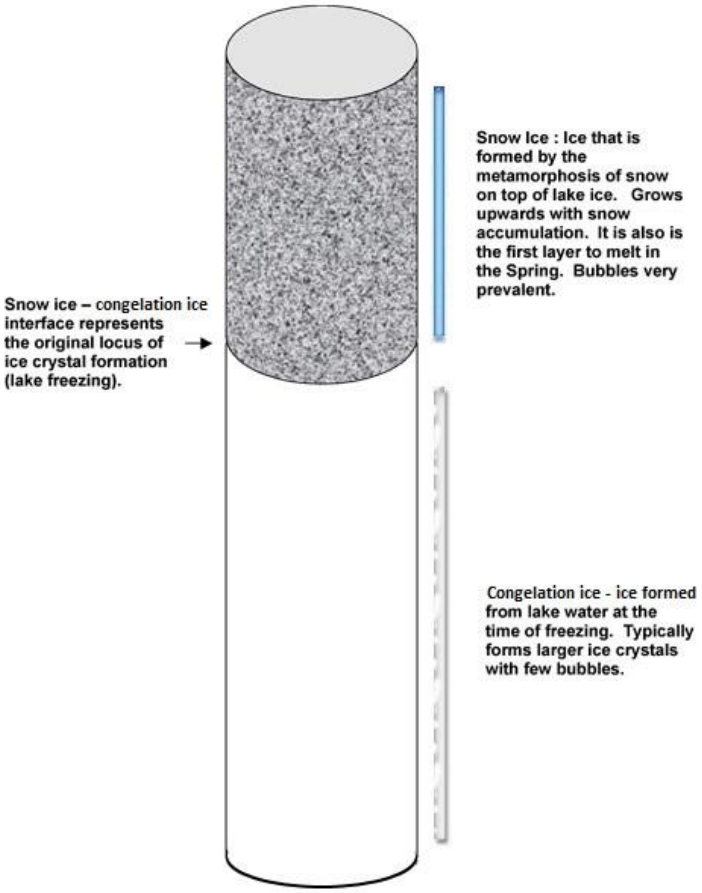

Figure 1.1.1: Schema of two types of lake/pond ice (www.blueiceonline.com)

Lake and pond ice cover has distinctive stratigraphic and crystalline structures, which can furnish useful information on the freezing history of the water and the crystallization process (Ashton, 1986). Ice has a hexagonal crystal structure with three identical a-axes in the basal plane and c-axis perpendicular to that basal plane (Durand et al., 2006). Orientation of crystal c-axes develops as the ice cover thickens. In some ice covers c-axis vertical crystals become dominant, in others, c-axis horizontal dominate. It was suggested that preferred orientation depends either on the thermal characteristics of the water body or on whether ice is seeded, formed by heterogeneous nucleation (Müller-Stoffels et al., 2008). Analysis of c-axis orientations performed by Müller-Stoffels et al. (2008) showed that preferred orientation become dominant in unseeded and seeded experiments, regardless of the air temperature and initial temperature of the water. The main result was that, when water freezes in calm

conditions, and unseeded ice covers form by spontaneous nucleation, c-axis vertical crystals become dominant, in contrast, in seeded ice formed by heterogeneous nucleation, c-axis horizontal crystals become dominant.

1.1.1 Thin section

The crystal orientation is determined by studying thin sections of ice, which provide a 3-dimensional characterization of ice crystals (Ashton 1986; Durand et al., 2006).

The thin section is made by cutting ice cores vertically or horizontally into very thin layers, approx. 0.3 mm thick, allowing light to pass through them. When thin sections are placed between two crossed polarization filters on a light table, the individual ice crystals can be seen (Durand et al., 2006; Gay and Weis, 1999).

Bubble-free ice is optically transparent, doubly refracting, uniaxial and optically positive. The colors of crystal (associated with birefringence) depend on their orientation (Ashton, 1986). The speed of light is different along the c-axis and the a-axes. This fact together with the orientation of the axes in a sample and the thickness of the sample will determine how the crystals look in polarized light. Ice crystals with vertical laying c-axes appeared in black; diagonal or horizontal laying crystals appeared in interference colors. The thickness of the ice sample is an important parameter for the grain boundary determinations (Durande et al., 2006; Hertl and Vikhamar, 1999).

Vertical and horizontal thin sections of ice in polarized light are seen in Figure 1.1.1.1 and 1.1.1.2. Figure 1.1.1.1 shows the vertical thin section of congelation ice composed of columnar crystals, and fine-grained snow ice above. Figure 1.1.1.2 shows the horizontal thin section of columnar crystal structure of congelation ice.

I took these photographs during the NASA History of Winter[1] 2013. The thin sections of ice were prepared as described in chapter 1.1.2 Sample preparation for thin section analysis. All work was done outdoor, where the temperature was about -10°C, so the ice structure didn't change during the preparation.

[1] The weeklong program for elementary and secondary science teachers regularly held each February since 2001 in Lake Placid, New York, USA. It brings together teachers and learning professionals from around the United States to study snow (in the air and on the ground), ice (crystal structure and axial orientation) and the winter ecosystem (interaction of the cryosphere and the greater environment) through intensive classroom and fieldwork exercises led by experts in the field.

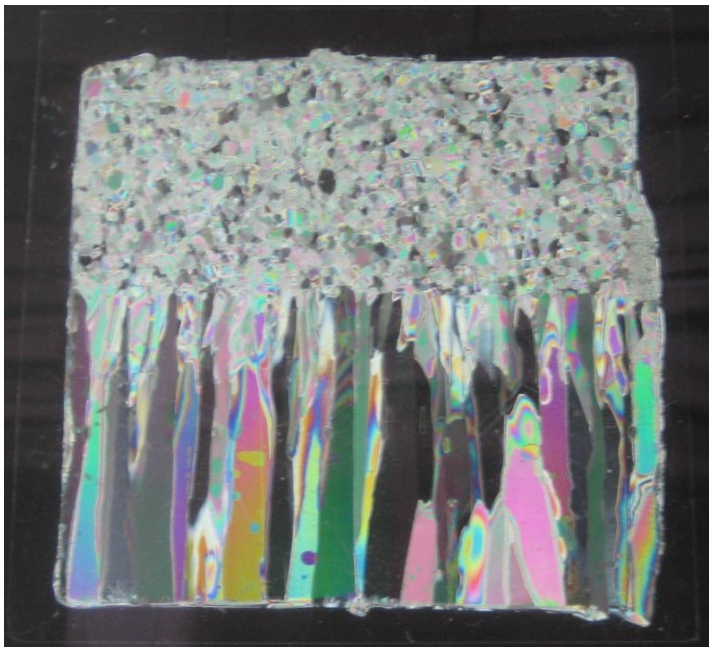

Figure 1.1.1.1: Vertical thin section of ice – congelation ice composed of columnar crystals exhibiting horizontal c-axes is overlaying by fine-grained snow ice. Thickness of the section is a fraction of millimeter. Black color indicates crystals with c-axis vertical, interference colors indicate diagonal or horizontal laying crystals.

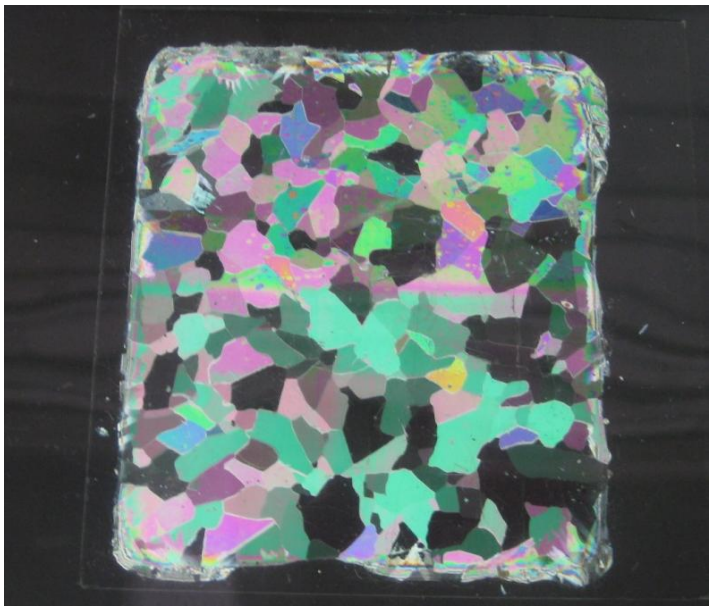

Figure 1.1.1.2: Horizontal thin section of columnar crystal structure of congelation ice. Thickness of the section is a fraction of millimeter. Vertical laying c-axes crystals appeared in black, diagonal or horizontal laying crystals appeared in interference colors.

1.1.2 Sample preparation for thin section analysis

To prepare a thin section of ice, first a vertical (parallel to the core axis) or a horizontal (perpendicular to the core axis) thick section about several centimeters in thickness is cut from the ice core. One surface of this sample has to be flattened in order to obtain a plane surface. It can be done by sandpaper or by placing thick section on a glass plate, with a few drops of water along its side to glue it to the glass plate. The plate is fixed to a microtome and is shaved in order to produce a smooth and plane surface. Then, the sample is removed from the glass plate by breaking the water frozen droplets with a cutter. The smooth flat ice surface is placed onto the surface of glass plate that has been warming on a slide warmer. The warm glass causes the ice face to melt and when removed from the warmer and placed in a freezer or cold air the water will freeze and so the sample of ice is glued to the glass surface. Using a band saw, the sample is cut parallel to the glass plate leaving between 1 and 2 mm thick section of ice adhering to the glass. Next the microtome knife is used to shave the ice to the desired thickness (about 0.3 mm) (Durand et al., 2006; Gay and Weiss, 1999; Langway, 1958).

1.2 Bubbles in ice

Natural ice is rarely a single-phase material. It generally contains chemical impurities and dust, as well as gas inclusions (Roessiger et al., 2012) – bubbles. The bubbles and their presence in ice affects the thermal, mechanical, optical and other physical properties of the ice cover (Heron, 1983).

The occurrence of bubbles in ice relates to gas content in the lake/pond water prior to freezing over the surface. The gas content in ice is limited by the gas solubility in water (Inada et al., 2009). The solubility in water increases with increase of gas pressure and decrease of temperature (Bari and Hallett, 1974). Gases are more soluble in water than in ice[2], so as water freezes to ice, dissolved gases, too large to fit into the lattice of ice, are rejected and redistributed at the ice-water interface (the surface between ice and water (Madrazo et al., 2009)), giving a saturation ratio in the water which increases with time and is a maximum at the interface (Inada et. al., 2009; Bari and Hallett, 1974). As freezing progresses, the concentration of dissolved gases surpasses a critical value, the water at the interface becomes supersaturated, and gas bubbles nucleate and grow to a visible size (Bari and Hallett, 1974; Carte, 1961; Maeno, 1967; Yoshimura et al., 2008) along the interface. Bubbles formed in this way can be found in lake and pond ice, and in hailstones (Bari and Hallett, 1974).

[2] In water at 0°C, the molecular solubility is 2 air molecules in 10^5 water molecules (3% by volume); in supersaturated ice, it is ≈0.6 molecule to 10^5 water molecules (Bari and Hallett, 1974).

Assuming that the gas bubbles are generated by homogenous nucleation (although they are generated heterogeneously) at the solid-liquid interface in most cases, the critical concentration c_n for the nucleation of gas bubbles is a linear function of the ambient pressure p, and is expressed as

$$c_n = c_{eq} + c_{n0} = \frac{p}{H} + c_{n0} \quad (1)$$

where c_{eq} is the equilibrium concentration of the dissolved gas in the water, H is the Henry´s law constant in units of Pa m^3/mol, and c_{n0} is the critical concentration of the dissolved gas for bubble nucleation when p approaches 0 (Yoshimura et al., 2008).

Gas bubbles are formed as a result of heterogeneous nucleation. As expected from the nucleation theory, some kind of nucleus must be necessary to form gas bubble (Maeno, 1967). Water of lakes and ponds usually contains a number of particles of a different substance, which may become centers of gas-bubble formation (nucleus) at relatively low supersaturations. Gas bubbles are formed at the ice-water interface on the surfaces of these centers (Maeno, 1967; Zhekamukhov, 1976). The nucleation sites may be provided by the air adsorbed or trapped on the surfaces of solid particles, or by the ice water interface, if is not kept so smooth that there are no irregularities, and grain boundaries act as the nuclei (Maeno, 1967). Bari and Hallett (1974) reported as the growth rates when the ice-water interface is flat, descent rates less than 5 μm s^{-1}. For larger growth rates, the interface becomes curved (Bari and Hallett, 1974). According to Yoshimura et al. (2008) roughness of the ice-water interface increased with increasing the pressure and with decreasing the growth rate.

Determination of supersaturation of gas solutions in water at ice-water interface with consideration of the kinetics of bubble formation is associated with many difficulties. In part these difficulties are connected with the fact that the number of active bubble-formation centers and the dependence of the activity of these centers on the degree of supersaturation of the gas solution are not known beforehand (Zhekamukhov, 1976).

The bubbles generated at the ice-water interface are either incorporated into the ice crystal as the ice-water interface advances, thus forming gas pores in the ice, or released from the interface (Inada et. al., 2009; Yoshimura et al., 2008). If there is incorporation or release is determined by several factors, such as the ice crystal growth rate, diffusion coefficient of the dissolved gas in water and in ice, the interaction forces between the bubbles and the solid ice crystal, the difference in thermal conductivity between the liquid water and the bubbles, and Marangoni effect[3] at the water-gas interface. Incorporation of bubbles

[3] The Marangoni effect is the fluid flow resulted from the gradient of surface tension. The presence of a gradient in surface tension will naturally cause the liquid to flow away from regions of low surface tension. The surface tension can be caused by concentration gradient or by a temperature gradient (Wu and Chung, 2011).

into ice crystals can be effected by ambient pressure. However, only a few studies using water ice crystals have reported this effect (Yoshimura et al., 2008).

The bubbles nucleated at the advancing ice-water interface may be characterized by concentration, shape, and size. The concentration and size of bubbles in ice depends on growth rate of ice, the amount of gases dissolved in water, and the particulate content of the water (Bari and Hallett, 1974; Carte, 1961). Such studies showed that the rate of ice growth affects the size, shape and distribution of bubbles and the porosity of the ice (Bari and Hallett, 1974; Carte, 1961; Zhekamukhov, 1976). This result was generally confirmed by the field study of Gow and Langston (1977). With increase of ice growth rate, the bubble concentration in ice increases and their sizes decreases (Bari and Hallett, 1974). In low rates, less and bigger bubbles are formed, in high rates, more and smaller bubbles are formed (Madrazo et al., 2009). Very low freezing rates give clear ice without bubbles (Bari and Hallett, 1974), the gases are able to diffuse and dissolve in the water reservoir (Boereboom et al., 2012), before they are enclosed in ice. Ice with no visible bubbles can be also observed when water is agitated by wind or artificial means (Yoshimura et al., 2008).

1.2.1 Other types of bubbles in ice

In contrast to bubbles nucleated at the advancing ice-water interface, graupel and glacier ice contain many inclusions trapped during consolidation of individual cloud drops or snow crystal (Bari and Hallett, 1974). Neither all air bubbles observed in lake/pond ice cover originate by rejection of gas at the ice-water interface. Occasionally, sediments or springs at the bottom of a pond or lake evolve bubbles of gas which, on rising to the underside of the ice sheet, become incorporated during freezing. Such bubbles are characteristically flattened by pressure against the underside of the ice, and this feature, in conjunction with their generally large size, serves to distinguish these accidental inclusions from bubbles produced by normal rejection of gas at the freezing interface (Gow and Langston, 1977).

1.2.2. Gas content of bubbles in ice

The bubbles in ice may be considered as enclosures filled with gas which was dissolved in water (Maeno, 1967). In general, the solubility of a gas in water at constant temperature is proportional to the pressure, in atmospheres, of the gas phase in contact with the water. This thermodynamic relationship for solubility of gas in liquid at constant temperature is called Henry´s law. For a mixture of gases, the effective pressure of each component is proportional to its fraction, by volume, in the mixture (Hem, 1989). The molal solubility (moles of gas per kilogram of solvent) relationship may be written as

$$(aqueous\ gas) = p/K_h \tag{2}$$

where *( )* represents molality, K_h is proportionality constant in units of moles kg^{-1} atm^{-1} (Henry´s constant) , and *p* is partial pressure of the gas. Henry´s constant is a function of temperature and pressure (Alley, 1993).

The amount of gases present in water is determined by three main factors: wind mixing that brings water into contact with the atmosphere; the biological activity that consumes or produces gases within a lake/pond; and gas composition of groundwater and surface water entering a lake/pond (Boereboom et al., 2012). Work of Boereboom et al. (2012) describes gas composition, total gas content and bubbles characteristics in lake ice cover of four adjacent lakes in a discontinuous permafrost area. The gas mixing ratios (for O_2, N_2, CO_2, and CH_4) suggested that gas exchange occurs between the bubbles and the water before entrapment in ice. Methane is produced within lake sediments as a result of acetate fermentation or CO_2 reduction in anaerobic conditions. During winter bubbles of methane are enclosed in the ice indicating that methane emission from sediment is an active process. The transit in the water column can induce several biochemical reactions. Methane can be oxidized to CO_2 in oxic conditions, via methanotrophic bacteria. Stratification of lakes favours the development of an anoxic layer whereas overturning causes oxygenation in the water column. Lakes are mainly stratified during the winter and the ice cover limits atmosphere-water interactions. This closed system results in the buildup of CO_2 and CH_4 concentrations in the water and mixing ratios in the ice (Boereboom et al., 2012).

Comparison of Boereboom et al. (2012) between lakes enabled them to identify two major bubbling events shown to be related to a regional drop of atmospheric pressure. Further comparison demonstrated that winter lake gas content is strongly dependent on hydrological connections – according to their closed/open status with regards to water exchange, lakes build up more or less gases in their water and ice cover during the winter, and release it during spring melt (Boereboom et al., 2012).

Dissolved gases in natural waters differ in their origin. The composition of gases connected with the exchange processes between water and atmosphere depends mainly on their content in the atmosphere. In terms of abundance of gases in the Earth´s atmosphere, nitrogen, oxygen, argon and carbon dioxide account for 99.9% of the composition. Other gases present in water are methane, and, to a lesser extent, hydrogen sulfide, ammonia and heavy hydrocarbons (Nikanorov and Brazhnikova, 2004).

Oxygen is the most important of the gases in water, since most aquatic organisms need it to survive. It gets into water by diffusion from the atmosphere and the photosynthetic assimilation of aquatic plants and algae. Carbon dioxide, like oxygen, is affected by photosynthesis[4], respiration (basically the reverse of the photosynthetic reaction)

[4] Photosynthesis takes place in green plants, algae, cynobacteria and photosynthetic bacteria where the sunlight is converted into chemical energy. In green plants photosynthesis requires, besides light as the energy source,

and contact with the atmosphere. Nitrogen comprises 78% of the gas in the atmosphere. Like other gases, it is more soluble at lower temperatures (Shaw et al., 2004). In waters, nitrogen occurs in various oxidation states, in ionic and non-ionic form (Pitter, 1999). Chemical and biological processes that transfer nitrogen to and from hydrosphere (lithosphere, atmosphere and biosphere) represent the nitrogen cycle (Hem, 1989). Hydrogen sulfide and methane gas may form under anaerobic conditions and disperse into lake/pond water from underlying sediments (Shaw et al., 2004). Volcanic processes and degassing of the Earth´s mantle supply oxides and dioxides of carbon, methane, ammonia, hydrogen sulfide, hydrogen, hydrogen chloride, sulfurous gas and others into natural waters. Some other gases can appear and dissolve in water as a result of ultra-violet irradiation (ozone), thunderstorm discharges (nitric oxide), and anthropogenic pollution (sulfurous gas, vapors of iodine, ammonia, carbonic oxide, etc.) (Nikanorov and Brazhnikova, 2004).

The gas composition of bubbles in ice is close to the composition of gas dissolved in water. But the gas composition in the bubbles depends on the diffusion coefficient of the gas components in water (Berner et al., 1977).

Continued from page 9 only two raw materials: water and carbon dioxide from the atmosphere. The organic compounds produced by photosynthesis, directly or indirectly, include sugar, carbohydrates, lipids and proteins. The overall biochemistry of photosynthesis for the formation of one glucose molecule from six CO_2 molecules may be written as:

$$6\ CO_2 + 12\ H_2O + 18\ ATP + 12\ NADPH \rightarrow C_6H_{12}O_6 + 18\ ADP + 18\ P_i + 12\ NADP^+ + 12\ H^+ + 6\ O_2\uparrow.$$

The essential photochemical process includes the decomposition of water into oxygen, which is released to the atmosphere, and the generation of reducing power in the form of NADPH, plus ATP, a principal energy currency formed from ADP by a photosynthetically generated proton gradient, both of the latter two species contributing to the biosynthesis of carbohydrates and other compounds. Biosynthesis of carbohydrates from carbon dioxide occurs via the Calvin cycle. The formation of a six-carbon sugar molecule requires six complete turns of the Calvin cycle, for each of which three ATP and two NADPH molecules are consumed (Bacon, 2001).

Gas	Mole Fraction Solubility / 10^{-5}
H_2	1.411
D_2	1.461
He	0.70797
Ne	0.82226
O_2	2.3011
NO	3.477
N_2	1.1774
CO	1.7744
Ar	2.5319
CH_4	2.5523
Kr	4.5463
O_3	9.1
CO_2	61.48
N_2O	43.67

Table 1.2.2.1: Mole fraction solubility of selected gases in water at 298.15 K and 101.325 kPa partial pressure of gas (modified after Scharlin et al., 1998)

1.2.3 Shape of bubbles

Previous studies reported that when the bubbles are incorporated into the ice crystal, they typically appear egg-shaped or elongated cylindrical (Bari and Hallett, 1974; Madrazo et al. 2009; Yoshimura et al., 2008). As mentioned earlier, the shape of bubbles is affected mainly by rates of ice growth. Low rates give bubbles usually with an egg shape; in high rates bubbles with shape of cylinder are formed (Madrazo et al., 2009).

Bari and Hallett (1974) investigated experimentally nucleation and growth of bubbles during freezing of solution of air in water using different techniques to give freezing rates between 1 μm s^{-1} and 10 mm s^{-1}. They carried out several types of experiment. Distilled water, passed through an ion exchange column, was used for all studies. The water was bubbled with filtered air.

In an experiment of Bari and Hallett (1974) with changing freezing rate, the maximum growth rate occurred at the beginning of freezing and was about 80 μm s^{-1}. Large numbers of small egg-shaped bubbles formed with the narrow end pointing in the freezing direction. At a growth rate of about 25+/- 1 μm s^{-1}, some cylindrical bubbles formed with their axis along the direction of freezing, gradually replacing egg-shaped bubbles, which cease at 5+/-1 μm s^{-1}. Simultaneous occurrence of cylindrical and egg-shaped bubbles was observed at 18 μm s^{-1}. Cylinders ceased entirely at a growth rate of 3+/-1 μm s^{-1}, to give completely clear ice. Bubbles were not arranged randomly in space. They showed some periodicity. Bubbles tend to occur in layers perpendiculars to the growth direction. Even without agitation some bubbles were released during freezing and rose to the surface of the water. This occurred only with freezing rates less than about 20 μm s^{-1} (Bari and Hallett, 1974).

Scheme of apparatus used by Bari and Hallett (1974) to investigate nucleation and growth of bubbles during freezing with changing freezing rate is redrawn in Figure 1.2.3.1 from their Figure 1. In this case, upward freezing was performed. In the water convective motions do occur caused by vertical temperature gradients; the region from 0 to 4 °C will be convectively unstable because of the upward increase of density of the water. In order to investigate this effect, Bari and Hallett (1974) studied freezing also vertically downward by the apparatus redrawn in Figure 1.2.3.2 from their Figure 8. The results showed essentially the same structure as that obtained with upward freezing. Bubble layers were flatter and somewhat more distinct. All air bubbles were trapped in the ice (Bari and Hallet, 1974).

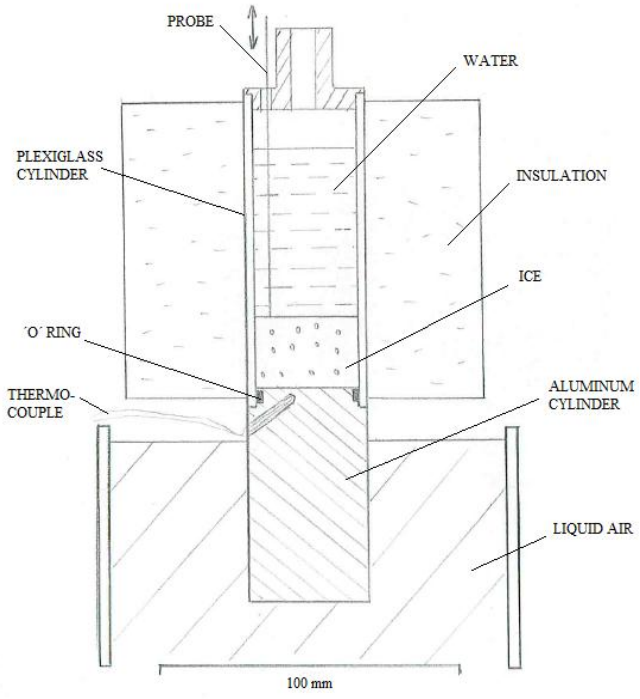

Figure 1.2.3.1: Growth apparatus for upward freezing, varying growth rate (Bari and Hallett, 1974)

Constant growth rate experiment was used to investigate the effect of insoluble suspended particulates on the bubble nucleation. At low growth rates, bubbles were typically of millimeter dimensions. Air bubble concentrations depended critically on growth rate, initial air concentration, and the particulate content of the water. For growth velocities of 1.5 μm s^{-1} or less, the ice was visually clear. Bubbles nucleated at greater growth velocities, with concentration increasing with initial air concentration and particulate content of the water. As in variable freezing rate study, air bubbles were either cylindrical or egg-shaped. Occasionally cylinders or lines of cylinders occurred over the whole range of growth rates studied. A few egg-shaped bubbles occurred mostly at slower growth rates. Small 100 μm wax particles deposited at the growing ice-water interface gave rise to lines of bubbles, either spherical or in the form of short cylinders (Bari and Hallett, 1974).

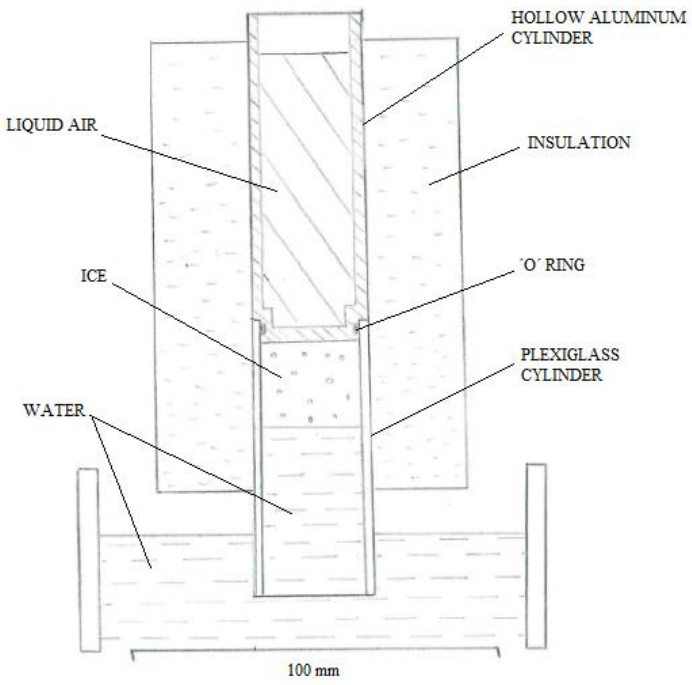

Figure 1.2.3.2: Growth apparatus for downward freezing, varying growth rate (Bari and Hallet, 1974)

Yoshimura et al. (2008) reported as the first the effect of pressure on the shape of the incorporated bubbles in ice. They experimentally and theoretically investigated structural features of oxygen gas bubbles incorporated into a growing ice crystal at various ice growth rates and ambient pressures. Four patterns of the shapes of bubbles were observed within the experimental conditions used in the study: a) egg-shaped bubbles, b) egg-shaped bubbles and cylindrical bubbles, c) cylindrical bubbles, and d) bifurcated cylindrical bubbles.

These four patterns were mapped out as functions of the ice growth rate and ambient pressure. The average diameter and interval (distance between them) of the cylindrical bubbles were measured as functions of the growth rate and ambient pressure. Both the measured diameter and interval decreased with increases in either the growth rate or ambient pressure. The changes in the patterns according to growth rate and pressure were following: at constant pressure, the egg-shaped bubbles became dominant with increasing growth rate, whereas at constant growth rate, the cylindrical bubbles became dominant with increasing pressure (Yoshimura et al., 2008).

Gas bubbles, nucleated at the ice-water interface, grow as far as the surrounding water is supersaturated. The supersaturation of gas is maintained by a continuous development of the ice-water interface. When the gas supply to the bubble is reduced or stopped, it may be enclosed in ice in the shape of an egg. When the gas supply is continuous and constant the bubble grows in the shape of cylinder (Maeno, 1967). The occurrence of these two distinct bubble forms can be seen as a competitive process. The supply of gas can be cut off by competition (Bari and Hallett, 1974); if another bubble nucleates nearby at the ice-water interface, the supply of the dissolved gas to the already existing bubble is reduced, and the already existing bubble stops extending (Yoshimura et al., 2008). At higher growth rates, saturation ratios at the ice-water interface are higher and more nuclei become activated, more bubbles form and then the probability of the competitive process increases (Bari and Hallett, 1974).

Yoshimura et al. (2008) reported that bubbles are incorporated in ice as egg-shaped bubbles and cylindrical bubbles of finite length. The finite length of the bubbles is probably due to the disturbance of the water-gas or ice-water interface. When the disturbance causes a slight decrease in the size (cap diameter) of a bubble located at the ice-water interface, the internal pressure of the bubble increases and thus the concentration of the dissolved gas at the bubble surface increases according to Henry´s law. The diffusion of the dissolved gas into the bubble decreases, and eventually the bubble stops extending, being completely incorporated in ice. As the growth rate of ice increases, the decrease in the size of the bubbles becomes more rapid, and the bubbles are more apt to be incorporated in ice as an egg-shaped or cylindrical bubble of finite length (Yoshimura et al., 2008).

The lines of bubbles (spherical or cylindrical) can be interpreted as caused by the migration of a nucleating particle along with the ice-water interface (Bari and Hallett, 1974). Most of the solid particles migrate with the advancing ice-water interface leaving these lines of spherical or cylindrical air bubbles in the ice. Lines of spherical bubbles can be also formed as a result of a thermal metamorphism of cylindrical bubbles (Maeno, 1967). In particular, cylindrical bubbles break up into individual elements, an effect which could lead to considerable uncertainty (Bari and Hallett, 1974). Details are described in the next section (1.2.4 Metamorphism of gas bubbles).

1.2.4 Metamorphism of gas bubbles

When ice becomes a subject of various thermal or mechanical disturbances, the contained gas bubbles may change their characters. The metamorphism of the bubbles involves the change in shape or arrangement and also in size. Metamorphism can occur under an isothermal condition due to exposure to a thermal gradient and/or a mechanical stress (Maeno, 1967).

The gas bubbles enclosed in ice tend to change their shapes. If the ice is kept for a long time near the melting point, gas bubbles shrink in size, suggesting some kind of diffusion process of defects in ice. Cylindrical gas bubbles split into smaller spherical ones (Maeno, 1967). At very low temperatures the cylinders may retain their shapes (Mullen and Warren, 1988). Under a very faint thermal gradient gas bubbles can undergo a metamorphism, forming solid ice crystals in them. The deformation of gas bubbles under stress or flow has been assumed to occur only following an increase of pressure inside them. However, the gas is able to diffuse into the surrounding ice, since the spacious lattice of ice may be distorted by the mechanical disturbance and create room for this gas (Maeno, 1967).

Maeno (1967) observed the metamorphism in cylindrical air bubbles whose diameters were less than 500 μ, but it was noted that larger air bubbles did not split easily. Significant metamorphosis of bubbles occurred after 10 h at -10 °C, cylindrical bubbles becoming unstable and forming a line of individual bubbles after 120 h (Bari and Hallett, 1974; Maeno, 1967).

1.3 Growth rate of ice, ice thickness

Once an initial layer of ice has formed at the lake/pond surface, further growth proceeds in proportion to the rate at which energy is transferred from the bottom surface of the ice layer to the air above (Ashton, 1986). The temperature of the ice-water interface is considered to be equal with the water freezing temperature (Liston and Hall, 1995). If there is no significant flow of heat (heat transfer) to the ice from the water below all the heat loss through the ice cover will result in ice growth at the bottom (Ashton, 1986).

The ice is added to the bottom of the layer of ice as heat is conducted upward through the ice (Mullen and Warren, 1988). The conduction of heat is proportional to the thermal conductivity of the ice and to the temperature difference between the bottom and the top surface of the ice, and it is inversely proportional to the thickness of the ice. Heat loss from the surface of the ice to the air above occurs by a variety of processes, including radiation and convection (Ashton, 1986).

Because the thermal conductivity of the ice is 1-2 orders of magnitude larger than that of the snow, any thickness of snow over ice provides a thermal barrier between temperature of the air and the temperature of the ice. The thickness of the ice over the lake or pond depends on how much snow covers the lake/pond (Kletetschka et al., 2013).

1.3.1 Stefan problem

The most commonly used method for predicting the thickness of ice is based on a simplified solution of the Stefan problem (Ashton, 1989). It applies not only to solidification, but also to melting. In one-sided Stefan problem only the heat field of one of the phases is taken into account (Madrazo et al., 2009).

The Stefan solution is based on the simple idea that the heat released by freezing at the ice bottom is conducted away through the ice by a constant temperature gradient. More precisely, Stefan´s solution is based on four assumptions:

a) No thermal inertia

b) No internal heat source

c) A known temperature at the top, $T_0 = T_0(t)$

d) No heat flux from the water (Leppäranta, 1993)

The Stefan solution is obtained by expressing the heat flux though the ice in the form

$$Q_i = -k(T_m - T_s)/h \tag{3}$$

where Q_i is the heat flux through the ice, k is the thermal conductivity of the ice, h is the ice thickness, T_m is the temperature at the ice-water interface (0° C) and T_s is the temperature of the top surface of the ice. T_s is taken as the air temperature (Ashton, 1989).

Stefan problem assumes that heat linearly conducted through the ice is exactly balanced by the latent heat of fusion of newly formed ice (Allison, 1979). The rate of the production of the ice at the bottom surface is

$$\rho L \frac{dh}{dt} = Q_i \tag{4}$$[5]

where L is the latent heat of fusion, ρ is the density of ice, and t is time (Ashton, 1989).

---

[5] This equation is derived by using assumption d) No heat flux from the water from the equation

$$\rho L \frac{dh}{dt} = k\partial T/\partial z|_{bottom} - Q_w$$

where Q_w is heat flux from the water to the ice. The boundary conditions are determined by the bottom temperature T_m and by the heat flux at the top surface Q_T, which is due to heat loss to (or gain from) the atmosphere and phase change.

Top: $k \frac{\partial T}{\partial z} = Q_m$

Bottom: $T = T_m$

The lower boundary level is not fixed but changes owing to melting and freezing (Leppäranta, 1993).

The expression for the ice thickness, *h*, after time t is then

$$h = \left(\frac{2k}{\rho L}\right)^{\frac{1}{2}} [\,(T_m - T_s)t]^{\frac{1}{2}} \tag{5}$$

(Ashton, 1989).

This relationship has often been used as the basis for the derivation of equations predicting growth of ice from air temperatures, although it has several serious limitations when applied to the growth of a real ice cover. Stefan problem makes no allowance for changes of heat content within the ice or for the time taken for surface temperature changes to vary the heat flux at the lower boundary. Other factors modifying the growth of ice cover may include the existence of other heat sources or sinks (for example, turbulent heat transfer between the ice, and underlying water or shortwave radiation absorption within the ice), variation of the thermal properties of the ice with depth and time, and the presence of a snow cover insulating the ice surface from the air temperature (Allison, 1979). In practice, data show that an additional empirical coefficient, α, usually in the range 0.5 - 0.8, must be applied to the right-hand side to give results as measured. Stephan solution then works well for thicker ice or very cold conditions but dramatically overestimates the growth rate of thin ice and less severe temperatures (Ashton, 1989).

1.3.2 Ashton solution

Ashton (1989) included to the Stefan solutions the effect of the thermal resistance between the top of the ice surface and the bulk temperature of the air. In addition to (3) and (4), the flux of heat Q_{ia} from the ice surface to the air above is expressed in the form of a bulk heat transfer coefficient H_{ia} applied to the difference between the top surface temperature of the ice and the air temperature above the ice, T_a, resulting in

$$Q_{ia} = H_{ia}\,(T_s - T_a) \tag{6}$$

Assuming that the heat flux through the ice equals the heat flux from the surface of the ice to the air above, then T_s may be eliminated using (3), (4) and (6). This results in

$$\frac{dh}{dt} = \left(\frac{1}{\rho L}\right)\frac{T_m - T_a}{\left(\frac{h}{k} + \frac{1}{H_{ia}}\right)} \tag{7}$$

This may be integrated, again with the boundary condition that $h = 0$ when $t = 0$ and results in expression for *h* in the form

$$h = \left[\frac{2k}{\rho L}(T_m - T_a)t + \left(\frac{k}{H_{ia}}\right)^2\right]^{\frac{1}{2}} - \frac{k}{H_{ia}} \quad (8)$$

For large values of the product $(T_m - T_a)t$, (8) converges to the form of (5), and ice growth is proportional to $t^{1/2}$. For small thickness ice growth is proportional to t but at a much lower rate than given by (4). To apply (8) in practical cases the bulk heat transfer coefficient must be estimated. One way of doing this is to apply detailed energy budget methods to the top surface of the ice, calculate the net transfer Q_{ia}, determine T_s, and then determine H_{ia} by dividing by the temperature difference $T_s - T_a$ (Ashton, 1989).

The exact value of the bulk transfer coefficient (H_{ia}) depends on the various components of the energy budget, but it usually falls between 10 and 30 W m^{-2} °C^{-1}. Higher values are associated with windy conditions and lower values with still air conditions, but, with other information unavailable, a value of 20 W m^{-2} °C^{-1} fits data on ice growth quite well (Ashton, 1986).

1.3.3 Other solutions

Liston and Hall (1995) reported a thermal energy balance at the ice-water interface that takes the form

$$\rho_i L_f \frac{dz_i}{dt} = (T_f - T_0)\left(\frac{z_i}{k_i} + \frac{z_s}{k_s} + \frac{z_m}{k_m} + \frac{z_w}{k_w}\right)^{-1} - h_w (T_w - T_f) \quad (9)$$

where ρ_i is the ice density, L_f is the effective latent heat, h_w is the convective-transfer coefficient, assumed to be 0.56 W K^{-1} m^{-2} for a calm lake based on conductivity considerations, T_f is the water-freezing temperature, T_w is the lake/pond-water temperature at the depth of 0.33 m, z_i is the ice depth, z_s is the snow depth, k_i is the thermal conductivity of the ice, and $\frac{dz_i}{dt}$ is the growth rate of the ice (Liston and Hall, 1995).

If it is assumed that the temperature of the air above the ice is equal to the temperature at the surface of the ice $(T_a = T_s)$ and that $T_a < 0$°C, equation of the estimate of the ice thickness obtained by the classic Stefan solution (5) can be written as

$$h = \sqrt{\frac{2kt^*}{\rho_i L}(DDF)} \quad (10)$$

where t^* is the number of seconds in a day, and DDF is degree-days of frost [°C day] defined as

$$DFF = 0.0 - \frac{(T_{max} + T_{min})}{2} \quad (11)$$

where T_{max} is the maximum daily air temperature [°C] and T_{min} is the minimum daily air temperature [°C]. The accumulated degree-days of frost *(ADDF)* can be used as a surrogate indication of the heat input-output at the site, commencing with freeze-over. Using the typical values, equation (12) can be generated by substitution

$$h = 3.47(ADDF)^{\frac{1}{2}} \tag{12}$$

where h is in [cm]. If, for example, the average daily temperature for a 7-day period was -15 °C, the *ADDF* would be 105. Theoretically, the maximum ice thickness would have been 35.6 cm if initiated on day 1 of this period. (3.47 is maximum theoretical ice growth parameter) This formula accounts for the heat loss needed to freeze that additional thickness. It does not, however, consider the heat reaching the base of the ice sheet from the underlying water. This equation applies to the growth of congelation ice (Hinkel,1983).

1.4 Description of the area

The pond Dolní Tušimy is located in Mokrovraty, Czech Republic (geographical coordinates: 49°48′24,889″N, 14°13′54,007″E). Map of Czech Republic and its location is shown in Figure 1.4.1.

1.4.1 Climatic conditions

The climate of the Czech Republic belongs to the Atlantic-continental area of the temperate climatic zone of the northern hemisphere. Air masses originating at central latitudes predominate. There are also fairly frequent penetrations of air masses of tropical and arctic origin. The alternation of air masses is connected with frequent passage of atmospheric fronts through the year (Pretel et al., 2001). The country´s natural environment is characterized by four alternating seasons. The average annual temperature varies in dependence on geographic factors from 1.0 to 9.4 °C. Local temperature conditions depend greatly on the elevation above sea level, the geographic coordinates and local geomorphological conditions, especially on the sun exposure of the terrain. Atmospheric precipitation is one of the most variable climatic features (Pretel et al., 2001; Voženílek et al., 2007).

According to the Köppen-Geiger climate classification[6] the area, where the pond Dolní Tušimy is located, falls into climatic region Cfb (Voženílek et al., 2007). The Cfb climate is

[6] The most frequently used climate classification is that of Wladimir Köppen, presented in its latest version 1961 by Rudolf Geiger. Köppen´s classification was constructed on the basis of five vegetation groups referring to the climate zones of the ancient Greeks. The five vegetation groups of Köppen distinguish between plants of the equatorial zone (A), the arid zone (B), the warm temperate zone (C), the snow zone (D) and the polar zone (E).

a warm temperate fully humid climate with the warmest month lower than 22°C over average and four or more months above 10°C over average (Kottek et al., 2006).

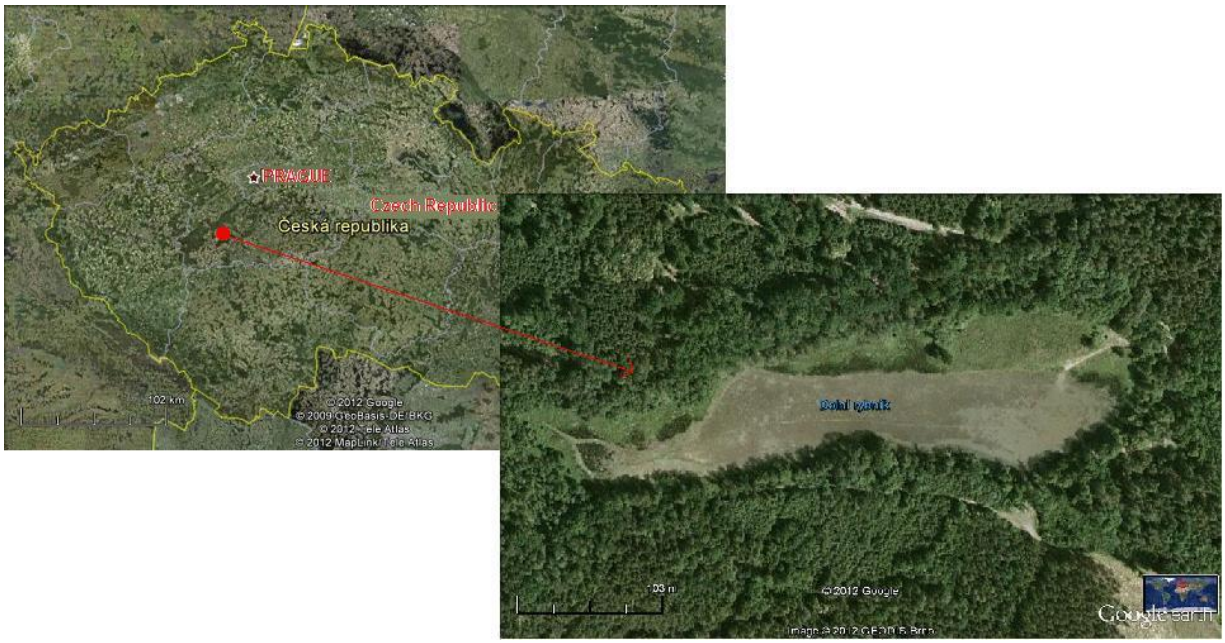

Figure 1.4.1 : Map of Czech Republic showing a location of the pond Dolní Tušimy. Yellow line is the state boarder of the Czech Republic. Red dot is the site location. This is Google earth image downloaded from internet on February 13, 2013.

1.4.2 Geology conditions

The territory of Czech Republic belongs to two distinct geological units – Bohemian Massif of Paleozoic origin and Outer Western Carpathians of Mesozoic to tertiary origin (Voženílek et al., 2007). The area of the pond Dolní Tušimy is a part of the Bohemian Massif, the Central Bohemian Region (Bohemicum) (Čech et al., 1994).

The Central Bohemian Region includes late Proterozoic and early Paleozoic complex cropping out in the central, western and eastern Bohemia and in western Moravia. Metamorphism is absent or very low-grade in the central part, progressively increasing towards the periphery. The rocks of the Central Bohemian Region continue as the basement of the Bohemian Cretaceous Basin up to the Elbe Line (Lusatian Fault and its southeastern continuation). The structure of the region is complex and several rather separate units can be distinguished (the Barrandian; the Metamorphic ‘‘Islets’’; the Domažlice Unit; the Teplá Unit; the Chrudim Paleozoic; the Železné hory Proterozoic; the Železné hory Pluton;

Continued from page 19 A second letter in the classification considers the precipitation, the third letter the air temperature (Kottek et al., 2006).

the Hlinsko Paleozoic and Proterozoic; the Polička Unit; and the Letovice Unit) (Čech et al., 1994).

The area of the pond Dolní Tušimy is located in the Barrandian unit. The Barrandian is regional geological designation of unmetamorphosed or slightly metamorphosed Proterozoic and Paleozoic (Cambrian to Devonian) rocks in central and south-western Bohemia, extending from the vicinity of Prague towards the SW as far as the town of Klatovy (Chlupáč, 1993). There are two principal tectonostratigraphic subunits: the Barrandian Paleozoic – sedimentary and volcanic rocks of Cambrian, Ordovician, Silurian and Devonian age, affected and consolidated by the Variscan orogeny (380 – 300 Ma); and the Proterozoic of the Barrandian, consolidated during the Cadomian orogeny (750 – 540 Ma) (Čech et al., 1994; Chlupač, 1993; Chlupáč et al., 2011; McCann, 2008).

The geology of the area of the pond Dolní Tušimy is displayed in Figure 1.4.2.1

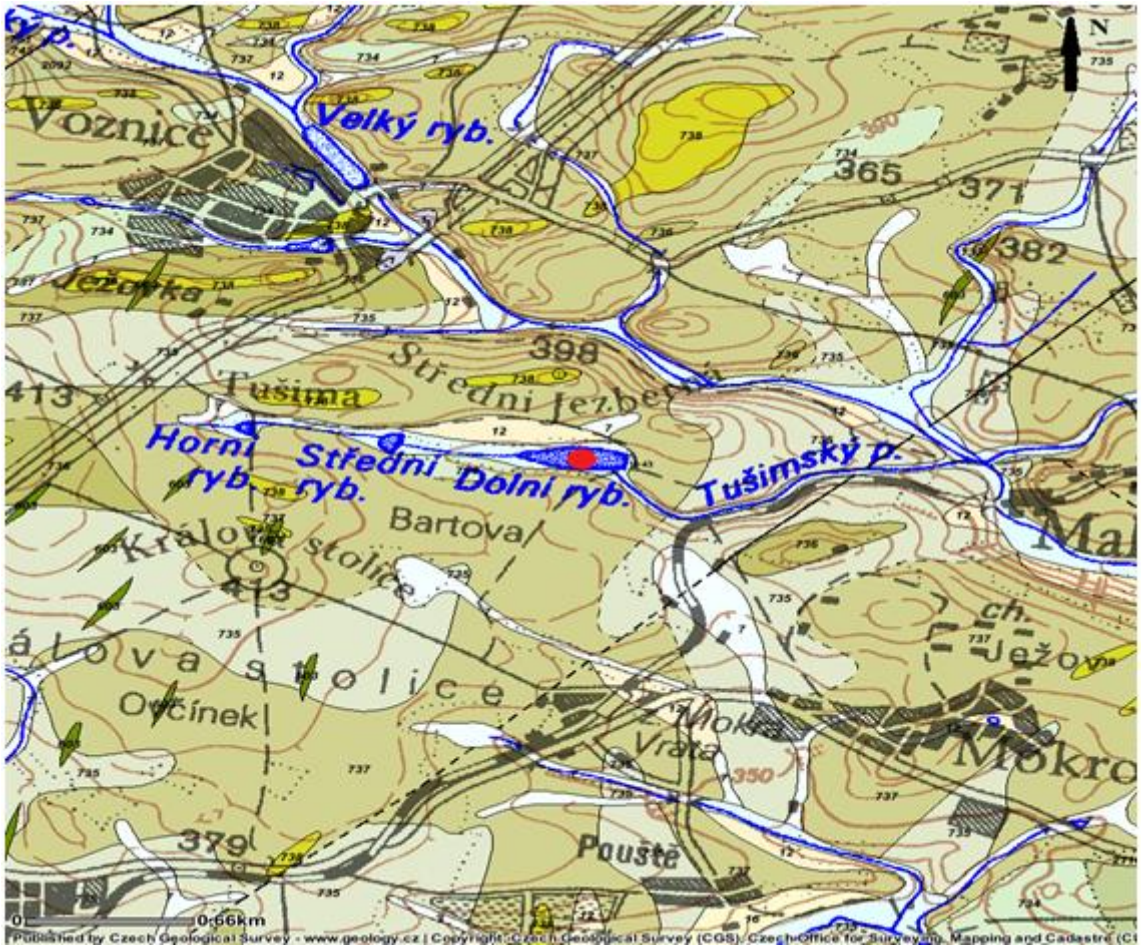

Figure 1.4.2.1: Geology map of the area of the pond Dolní Tušimy. The location of the pond Dolní Tušimy is marked by red dot .
(http://www.geology.cz/app/ciselniky/lokalizace/show_map.php?mapa=g50&y=759000&x=1073300&s=1)

Legend (translated from Czech:

http://www.geology.cz/app/ciselniky/lokalizace/show_map.php?mapa=g50&y=759000&x=1073300&s=1)

1.4.3 Description of the pond Dolní Tušimy

The pond Dolní Tušimy is the last (third) pond of a system on a tributary of the Voznický stream. It is a small; about 400 m long in EW and 60 m wide in NS directions, and its area is 4.12 hectares. The purpose of this pond is for landscaping, water budgeting, maintaining ecology, fish farming, and water storage, and for extinguishing the fire. Additional data are in support information (SI), hydrologic conditions: catchment area – 1.685 km², long-term average annual precipitation – 585 mm, long-term average annual flow – 3.0 l/s. Individual parts of the pond are: tank itself – a bottom, a dam, a drain device, a safety overflow and a littoral. The pond in question is a basin closed with the artificial dam equipped with the pipe secure system allowing draining the water out to prevent overfilling of the pond. The bottom of the tank is drained by a main pond sewer pipe line with a total length of 431.5 m and secondary sewer pipe line with a length of 42 m. Water level of the pond is

maintained at average depth of 1.28 m, and in case of secure overfilling system activation the average depth is 1,38 m (Fürst, 2005).

2. MATERIAL AND METHODS

2.1 iButton device

The iButton device is a computer chip enclosed in a 16 mm thick stainless steel can. Because of this unique and durable container, up-to-date information can travel with a person or object virtually anywhere. The steel iButton device is rugged enough to withstand extreme environmental conditions, indoors or outdoors, such as dirt, moisture, and shock (Hindman, 2006).

Each iButton device has a unique and unalterable address laser etched onto its chip inside the can. This address can be used as a key or identifier for each iButton device. Information is transferred between the iButton device and a PC with a momentary contact through a Blue Dot receptor or other iButton probe, which is connected to a PC. iButton device communicate through 1-Wire protocol (Hindman, 2006).

iButton varieties include: Address Only

Memory

Real-Time Clock

Secure

Data Loggers (Hindman, 2006)

iButtons are ideal for any application where information needs to travel with a person or object. They are small and portable enough to attach to a key fob, ring, watch, or other personal items, and be used daily for applications such as access control to buildings and computers, asset management, and various data logging tasks (Hindman, 2006).

Figure 2.1.1: iButtons and Blue dot receptor iButton reader cable

2.1.1 DS1922L Temperature loggers

The DS1922L temperature loggers iButtons are rugged, self-sufficient systems that measure temperature and record the result in a protected memory section (Keuschnig et al., 2012). Temperature recordings taken by the iButton are done at a user defined rate and a mission to collect data can be programmed to begin immediately, after a user-defined delay, or after a temperature alarm (http://datasheets.maximintegrated.com).

Main features of the DS1922L temperature loggers are listed below:

- Automatically wakes up, measures temperature, and stores values in 8KB of data-log memory in 8-Bit or 16-Bit format
- Digital thermometer measures temperature with 8-Bit (0.5 °C) or 11-Bit (0.0625 °C) resolution
- Accuracy of ±0.5 °C from -10 °C to +65 °C, with software corrections
- Water resistant or waterproof if placed inside iButton capsule
- Sampling rate from 1s up to 273 hr
- Programmable high and low trip points for temperature alarms
- Programmable recording start delay after elapsed time or upon a temperature alarm trip point
- 512 bytes of general-purpose memory plus 64 bytes of calibration memory
- Two-level password protection of all memory and configuration registers

- Communicates to host with a single digital signal up to 15.4kbps at standard speed or up to 125kbps in overdrive mode using 1-Wire protocol
- Operating temperature range: -40 °C to +85 °C

(http://datasheets.maximintegrated.com)

In contrast to conventionally used temperature loggers, iButtons are cheap, end user friendly and easily replaceable in case of damage (Keuschnig et al., 2012). The thermochron iButtons are most commonly used in temperature monitoring shipping of fresh food and pharmaceutical products and recently used for hydrogeology applications. It is a new tool for hydrogeologists because it collects high-resolution shallow water temperature data for a fraction of the cost and size of traditional temperature loggers (Ibrahim et al., 2009; Wolaver and Sharp, 2007). They are well suited for obtaining quality spatially distributed data for environmental investigations (Hubbart et al., 2005).

2.2 Method for measuring water and ice temperature

For the measurements of water and ice temperature in the pond Dolní Tušimy the autonomous temperature loggers iButtons (model DS1922L) were used. They were programmed using the OneWireViewer software to record the temperature every 30 minutes with a resolution of 0,0625 °C. The start of temperature recording was set on January 8, 7.00 PM. No rollover occurred. The iButtons were not calibrated prior to use and the clock of each sensor was synchronized to real PC time.

Seven of the DS1922L temperature loggers were sewn on a textile strip, as shown in Figure 2.2.1, with a rock of size about 5x5x9 cm and weight about 600 g tied at the end of it. The strip was attached to a wooden frame so the equipment was able to float (Figure 2.2.2). The stone at the end of the strip kept the devices in a vertical line beneath the water level.

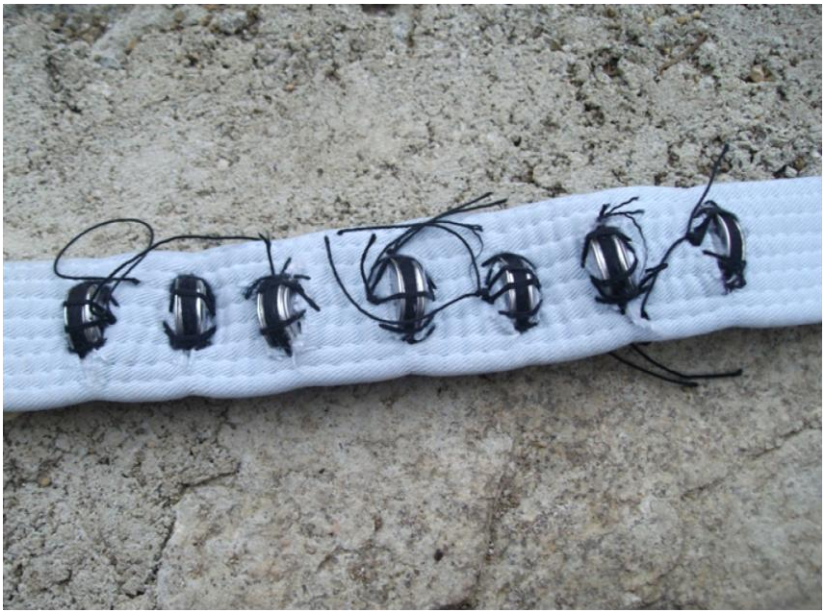

Figure 2.2.1: Textile strip with seven temperature loggers iButtons

This temperature measurement device was placed in the water of the pond Dolní Tušimy on January 8, 2012. There was no ice cover on that day over the pond and the wooden frame was floating on the surface with temperature loggers in the water. Their position was at a depth of 58 mm, 78 mm, 99 mm, 123 mm, 143 mm, 165 mm and 190 mm below the water level, so the temperatures were measured at these depths.

To keep the device in the same place in the pond there was a stake hammered in the bottom and the frame was anchored to it.

Figure 2.2.2: Temperature measurement device – floating wooden frame, textile strip with a stone at the end and temperature loggers

The period of temperature measurements lasted from January 8, 2012 to February 22, 2012. During this period, the air temperature dropped below freezing point (by January 25) and ice cover over the pond began to form.

Records of air temperatures were obtained from meteoradar, located 1.5 km northwest from the pond Dolní Tušimy (http://jmis2.jsdi.cz/arwis/smis/archive_big.php). These data serve as a meteo information for Road and Motorway Directorate of the Czech Republic (http://www.rsd.cz). Temperature was recorded about every five to six minutes with a resolution of 0.05 °C.

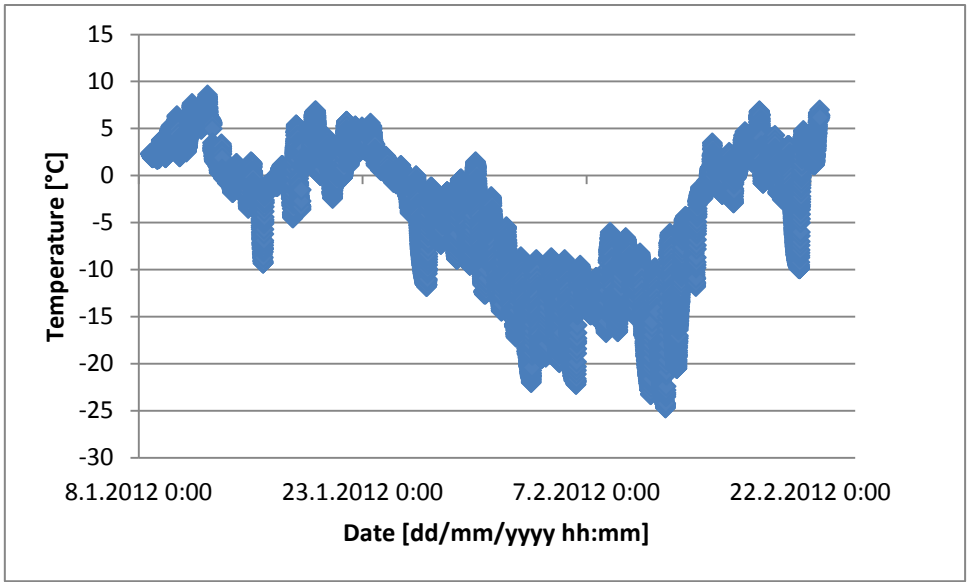

Figure 2.2.3: Record of air temperature, January 8 – February 22, 2012

2.3 Obtaining a sample of ice

At the end of the period of temperature measurements (on February 22, 2012) a sample of ice with the frozen temperature loggers in it were cut out using a hand saw. The sample of ice was triangular in shape with sides of length about 30 cm.

Several photographs of this sample of ice were taken for future investigation of ice structure. In order to highlight the structure, the ice was placed in the water of the pond, so dark background was formed, and then photographed.

The thickness of the ice cover was measured during the whole measurement period once a week and it attained its maximum of 28.5 cm about 12th of February. On that day when the sample of ice was taken, the thickness of ice was about 27.5 cm. These data were obtained by measurements taken from ice blocks that were cut using a hand saw.

Date [dd/mm/yyyy]	Thickness of the ice [cm]
14.1.2012	0.3
21.1.2012	4.9
28.1.2012	6.8
3.2.2012	17
12.2.2012	28.5
19.2.2012	28
22.2.2012	27.5

Table 2.3.1: Thickness of the ice

2.4 Data processing from temperature loggers

When the cut out part of the ice with the temperature loggers on strip began to melt in air temperature, the strip was pulled out and the sensors were removed from it. Data recorded by seven loggers were using the Blue dot receptor, 1-Wire adapter and the OneWireViewer software (version 0.3.15.50) transferred to PC and analysed using a Microsoft Excel 2007 program. Data included temperature in degrees Celsius and date in a form dd/mm/yyyy hh:mm. The time of sensors (that was synchronized to PC time prior use) differed (98 - 154 s) from PC time, when data were retrieved.

After loading data from the loggers to PC, it was found out that the sensor which measured the temperature in the depth of 190 mm didn´t work properly. It didn´t measure the real temperature and this record couldn´t be used for next study. Sensors in the depth of 58 mm, 78 mm, 99 mm, 123 mm, 143 mm and 165 mm worked properly.

Data retrieved from these six sensors included the period from January 8 to February 22. To illustrate the temperature changes the individual plots show one week period each.

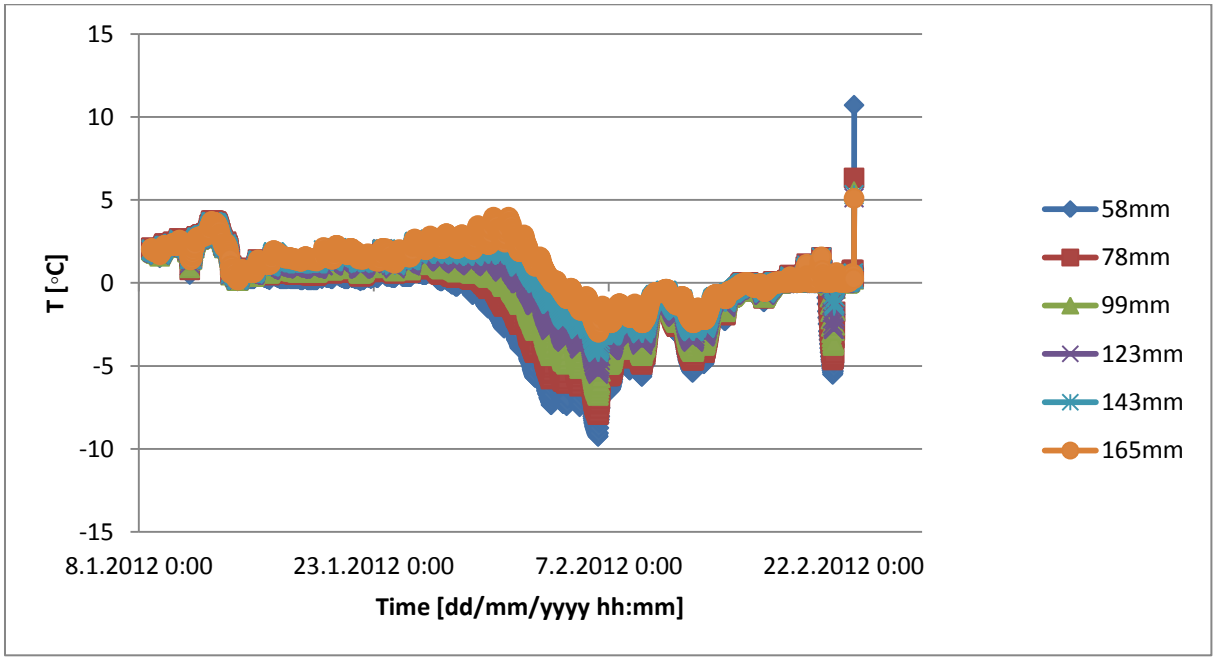

Figure 2.4.1: A complete record of temperature from six data loggers at depth of 58 mm, 78 mm, 99 mm, 123 mm, 143 mm and 165 mm below the water level , January 8, 2012 – February 22, 2012.

2.5 Determination of growth rates of ice from graphs

The determination of growth rates of ice from graphs will be shown on the example for the rate determined using data recorded by sensors in depths of 58 mm and 78 mm.

The first step was to find the time when the sensor in the depth of 58 mm was entirely within the ice. So its measured temperature was below freezing. For this case such time and temperature were: 29th of January, 15:30 and -0,004 °C.

The data used for a graph (Figure 2.5.1) included the temperature values recorded from 29th of January, 15:30 to such temperature values, when the curves of the graph seemed to be nearly linear.

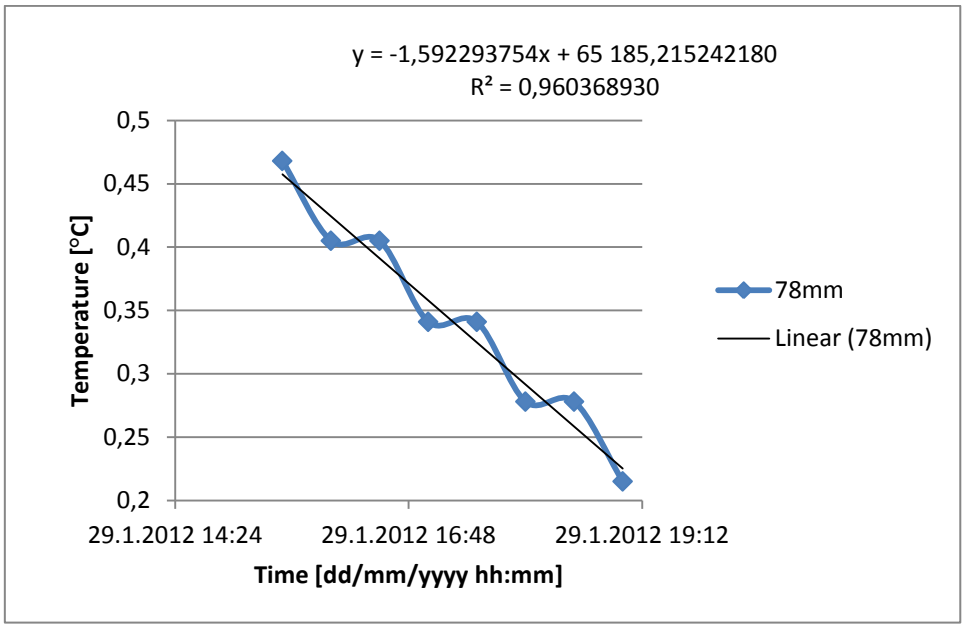

Figure 2.5.1:Temperature record from the sensor in the depth of 78mm, January 29, 15:30 – January 29, 19:00

The linear trendline was added to the chart and using the linear regression equation the time when the temperature would be 0 (y = 0) was determined. It was the time when the sensor in the depth of 78 mm would get into the ice, assuming still the same temperature gradient. This time was January 29, 22:23.

Then the times (January 29, 15:30 and January, 29, 22:23) for 0 °C temperatures for sensors in the depth of 58 and 78 mm were compared and it gave the difference 24780 s. The depth difference between sensors was 20 mm (78 mm minus 58 mm). These two values were used to calculate the growth rate of the ice in [mm/s].

The absolute error of the growth rate was calculated using the relative error of the temperature loggers +/- 0.003 °C. And the error of the depth was set as a half of vertical thickness of one sensor (+/- 3 mm).

3. RESULTS AND DISCUSSION

During analysis of individual graphs I focused on the period from January 28 to February 3 (Hrubá and Kletetschka, 2013). The formation of permanent ice cover of thickness exceeding 58 mm on the pond Dolní Tušimy did not begin until the 27th of January. Until this day temperatures recorded by all six sensors was above freezing and they were in water (not within ice).

The data for 7 days, from January 27 to February 3, are shown in Figure 8.1. During these days the temperature of all six sensors dropped below the freezing point (0 °C) and they successively became part of the ice as the ice thickened. The temperature of the logger at the depth of 58 mm plunged under 0 °C on January 27 and the 0 °C temperature at depth of 165 mm was reached on February 3.

Figure 3.1 shows daily temperature fluctuations with maximum values at about 2:00 PM, and minimum at about 7:00 AM. These are thermal responses from the air temperature. Layer of ice above the sensors provides a modified thermal insulation so the measured temperature was damped and delayed when compared with the air temperature.

Photographs of pond ice were analyzed for bubble formation. The layers of air bubbles were clearly distinct in the ice samples retrieved. Throughout the thickness of the ice about 13 layers of bubbles were noted. They were separated by approximately 2 cm layers of ice with low concentration of air bubbles that were arranged randomly in space.

As the incorporation of bubbles into the ice crystal is determined by the crystal growth rate and the concentration of bubbles increases with increase of the growth rate, the layers of bubbles may relate to high growth rates of ice. When comparing the temperature record and the photo of ice sample as shown in Figure 3.1, it is possible make an estimate when individual layers formed. In the parts of graph, where curves go quickly below 0 °C, the freezing progresses so fast, that the gases redistributed at the ice-water interface are not able to diffuse and dissolve again in water, and the bubbles of gas are enclosed in the ice.

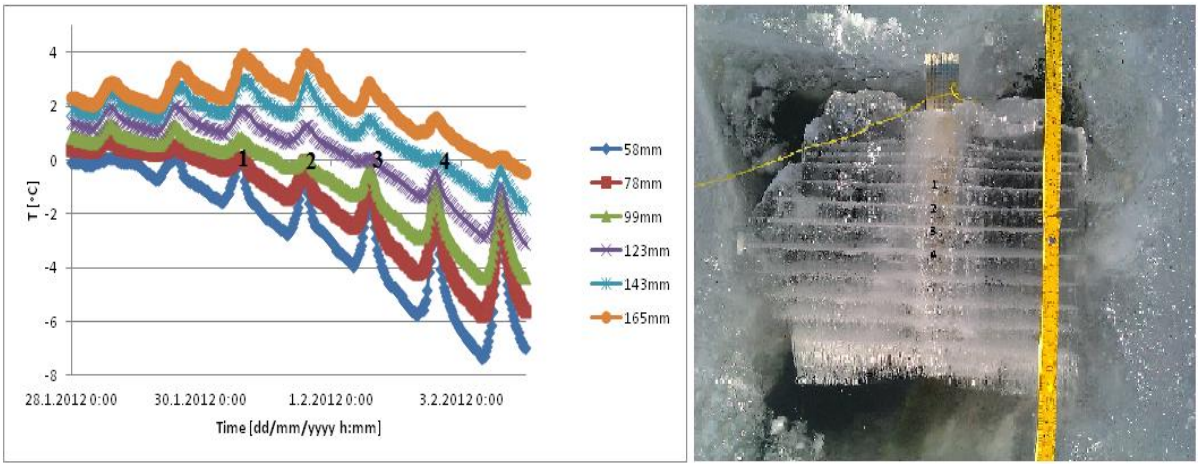

3.1: Comparison of the temperature record from six temperature data loggers and the photograph of the ice sample from the pond Dolní Tušimy.

Most studies reported that when bubbles are incorporated into the ice crystal they are typically egg-shaped or cylindrical. The egg-shaped bubbles become dominant with increasing growth rates and the cylindrical bubbles occur at lower growth rates. The shape of bubbles in the sample of ice from the pond Dolní Tušimy was mostly rounded. The size of bubbles forming layers was smaller than that of bubbles outside these layers. So the fact that the size of bubbles is also affected by rates of ice growth, and the size decreases with increasing rates was confirmed.

The bubbles of cylindrical shape occurred only on the bottom of the ice sample. It might be due to lower growth rates, as the layer of ice above provided a greater modified thermal insulation with increasing thickness. Cylindrical bubbles could be also formed because of the continuous supply of gas from the water of the pond with the bottom of ice was in contact.

Figure 3.2: Image of rounded and cylindrical gas bubbles in the ice cover of the pond Dolní Tušimy

The layers of bubbles can be interpreted as caused by the migration of nucleating particles along with the ice-water interface. Or layers of spherical bubbles could be formed as a result of a thermal metamorphism of cylindrical bubbles, which broke up into individual spherical bubbles.

Bari and Hallett (1974) stated as the ice growth rate which gives egg-shaped bubbles the rate about over 25 μm/s. Growth rates of ice less than that 25 μm/s gave cylindrical bubbles which ceased entirely at about 3 μm/s, to give completely clear ice. The maximum freezing rates for the pond Dolní Tušimy varied from 0.565 μm to 1.023 μm/s. The values of the growth rate of ice were determined from the temperature record of six temperature data loggers (as described in the chapter 2.5 Determination of growth rates of ice from graphs) and they are shown in Table 3.1.

Date [dd/mm/yyyy hh:mm]	**Growth rate [μm/s]**
29.1.2012 15:30	0.807 +/- 0.121
30.1.2012 16:30	1.023 +/- 0.147
31.1.2012 16:00	0.760 +/- 0.095
1.2.2012 16:30	0.565 +/- 0.085
2.2.2012 16:30	0.651 +/- 0.089

Table 3.1: The maximum growth rates of ice – the pond Dolní Tušimy

From Table 3.1 is seen that the growth rates of ice for the pond Dolní Tušimy are lower than those obtained experimentally by Bari and Hallett (1974). According to their results the ice covering the pond Dolní Tušimy would be clear without bubbles. This discrepancy (as also Gow and Langston, (1977) reported) may be related to the impurity content of the pond Dolní Tušimy. It is much greater than that of the distilled water used by Bari and Hallett (1974) in their experiments.

3.1 Comparison with the pond in Albertov

To compare the results obtained from the study of the ice cover over the pond Dolní Tušimy, temperature records and ice samples from other pond were analyzed. This pond is located at the university campus, in Albertov, Prague, Czech Republic.

Four temperature data loggers were used for the temperature measurements. They were programmed to record the temperature every 15 minutes with resolution of 0.5 °C, and their position was in the depth of 0, 40, 80 and 120 mm below the water level. The period of measurements lasted from December, 16 to February, 3 2012.

The photo of the sample of ice from the pond in Albertov is seen in Figure 3.1.1. When comparing this picture with the photo of the ice sample from the pond Dolní Tušimy it can be seen, that the bubbles in sample from the pond in Albertov were larger in size, their concentration was lower and they were arranged randomly in space. They didn´t form the distinct layers as could be seen in sample of ice from the pond Dolní Tušimy.

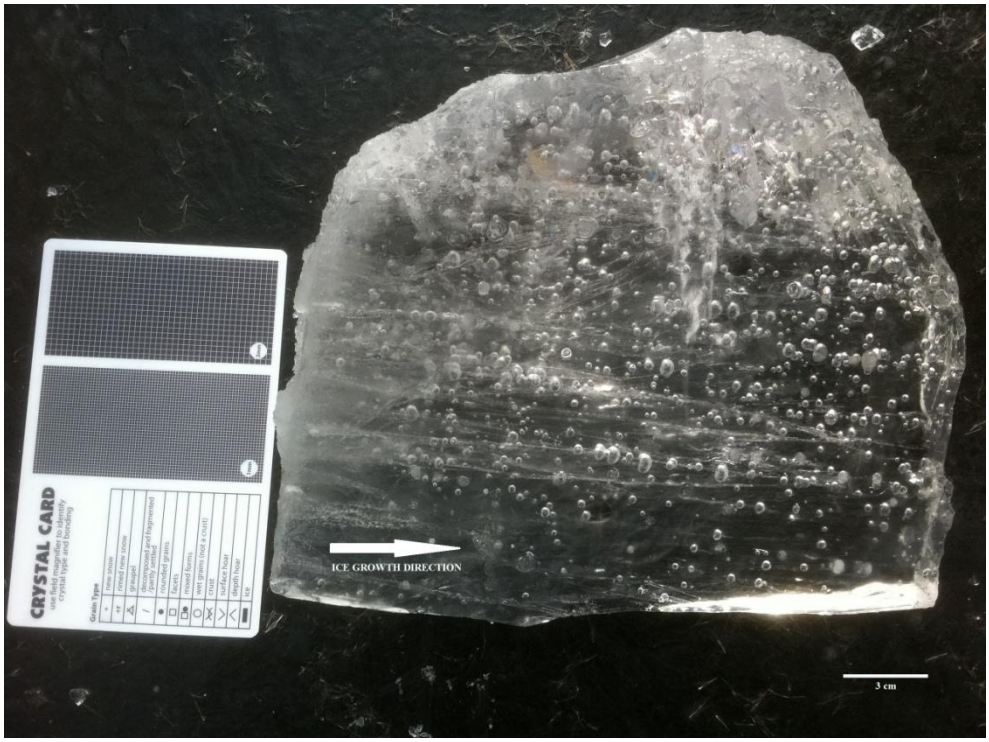

Figure 3.1.1: Sample of ice from the pond in Albertov

The Figure 3.1.2 shows the temperature records from one sensor from the pond Dolní Tušimy and from one sensor from the pond in Albertov. It is seen that black curve (temperature record from Albertov) is not so steep around 0 °C temperature. The ice cover over the pond in Albertov probably didn´t form so fast as the ice over the pond Dolní Tušimy. This fact also corresponds to the form and size of gas bubbles in the ice.

For the better comparison of temperature record from the Dolní Tušimy pond and the pond in Albertov, it would be best to also estimated growth rates of ice from the graph as for the pond Dolní Tušimy. But it could not be done because of the low resolution of recorded temperature.

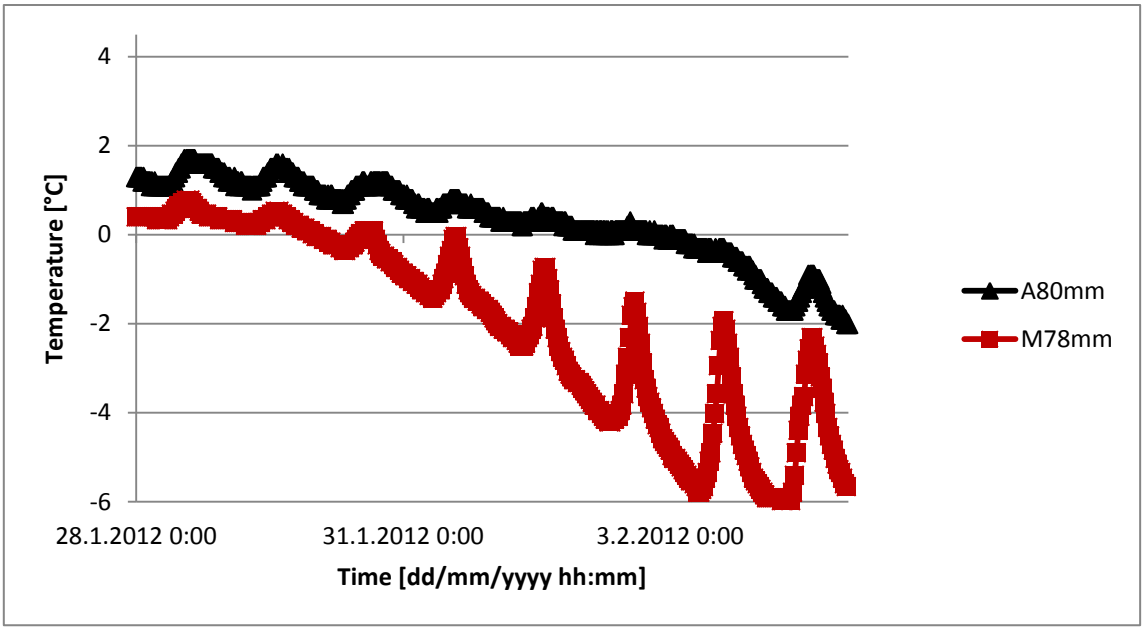

Figure 3.1.2: Temperature record: red curve – sensor in the depth of 78 mm – Mokrovraty, the pond Dolní Tušimy; black curve – sensor in the depth of 80 mm - Albertov

4. CONCLUSION

Ice over lakes and ponds has distinctive stratigraphic and crystalline structures, which can furnish useful information on the freezing history of the water and the crystallization. Natural ice is rarely a single-phase material and it generally contains chemical impurities, dust and gas bubbles.

Bubbles in lake/pond ice are usually formed at the ice-water interface as a result of heterogenous nucleation, and they can be characterized by size, concentration and shape. The features of bubbles depend on growth rates of ice, the amount of gases dissolved in water, and the particulate content of the water. The rate of ice growth affects the size, shape and distribution of bubbles and the porosity of the ice. With increase of ice growth rate, the bubble concentration in ice increases and their sizes decreases. In low rates, less and bigger bubbles are formed, in high rates, more and smaller bubbles are formed. Very low freezing rates give clear ice without bubbles.

The relation between growth rates of ice and the occurrence of the bubbles in ice was study on the ice formed under natural conditions over the pond Dolní Tušimy. Temperature of the water of the pond and the temperature of the ice were measured by temperature loggers iButtons. Characters of bubbles were analyzed from the ice samples.

The layers of gas bubbles were clearly distinct in the ice samples retrieved. They were separated by approximately 2 cm layers of ice with low concentration of air bubbles that were arranged randomly in space. Shape of bubbles was mostly rounded. The bubbles of cylindrical shape occurred on the bottom of the ice sample. They formed due to lower growth rates,

as the layer of ice above provided a greater modified thermal insulation with increasing thickness and because of the continuous supply of gas from the water of the pond with the bottom of the ice was in contact. The size of bubbles forming layers was smaller than that of bubbles outside these layers.

The layers of bubbles were caused by the migration of nucleating particles along with the ice-water interface, and they were related to fast growth rates of ice. Growth rates of ice were determined from the temperature records from data loggers. The maximum growth rates were about 1 μm/s.

The comparison with similar work done showed some distinction. Literature reported that when bubbles are incorporated into the ice crystal they are typically egg-shaped or cylindrical. The egg-shaped bubbles become dominant with increasing growth rates and the cylindrical bubbles occur at lower growth rates. The growth rates of ice for the pond Dolní Tušimy were very much lower than for example those obtained experimentally by Bari and Hallett (1974). According to their results the ice covering the pond Dolní Tušimy would be clear without bubbles. This discrepancy was probably related to the impurity content of the pond Dolní Tušimy that was greater than that of the distilled water used by Bari and Hallett (1974). The distinction was also caused due to different methods of ice formation (laboratory condition vs. natural conditions).

The results of this work confirm the relation between growth rates of ice and the occurrence of bubbles in ice. If the phase change of water into ice occurs rapidly, the growth rate of ice is fast, the concentration of bubbles incorporated into ice crystals is high and bubbles are small. During lower growth rates some bubbles nucleated at the ice-water interface are able to diffuse back to the water; the concentration of bubbles in ice decreases and the incorporated bubbles are bigger. Direct comparison of the results from bubble-containing ice formed under laboratory conditions to results from this study performed on the pond ice is not relevant.

5. REFERENCES

Alley, William M., (1993). Regional Ground-Water Quality. Van Nostrand Reinhold, New York, 634p.

Allison, I., (1979). Antartic sea ice growth and oceanic heat flux. Sea Level, Ice, ami Climatic Change (Proceedings of the Canberra Symposium, December 1979), IAHS Publ. no. 131, 161-170.

Ashton, George D., (1986). River and Lake Ice Engineering. Water Resources Publication, USA, 485p.

Ashton, George D., (1989). Thin Ice Growth. Water Resource Research, vol. 25, no. 3, 564-566.

Bacon, K., (2001). Photosynthesis, Photobiochemistry and Photobiophysics. Kluwer Academic Publishers, Dordrecht,763p.

Bari, S. A., Hallett, J., (1974). Nucleation and Growth of Bubbles at an Ice-Water Interface. Journal of Glaciology, vol. 13, no. 69, 489-520.

Bengtsson, L., (2012a). ICE COVERED LAKES. In Encyclopedia of Lakes and Reservoirs. Bengtsson, L., Herschy, R. W., Fairbridge, R. W., (eds.). Springer, Encyclopedia of Earth Sciences Series, 357-360pp.

Bengtsson, L., (2012b). ICE FORMATION ON LAKES AND ICE GROWTH. In Encyclopedia of Lakes and Reservoirs. Bengtsson, L., Herschy, R. W., Fairbridge R. W., (eds.). Springer, Encyclopedia of Earth Sciences Series, 360-361pp.

Berner, W., Bucher, P., Oeschger, H., Stauffer, B., (1977). Analysis and interpretation of gas content and composition in natural ice. In Isotopes and Impurities in Snow and Ice. Wallingford, Oxon., International Association of Hydrological Sciences, 272–284.

Boereboom, T., Depoorter, M., Coppens, S., Tison, J. L., (2012). Gas properties of winter lake ice in Northern Sweden : implication for carbon gas release. Biogeosciences, 9, 827–838.

Carte, A. E., (1961). Air bubbles in ice. Proc. Phys. Soc., 77, 757-768.

Čech, S., Chlupáč, I., Dudek, A., Eliáš, M., Holub, V., Pešek, J., Pouba, Z., Shrbený, O., Tyráček, J., Valečka, J., Vejnar, Z., Zapletal, J., (1994). REGIONAL GEOLOGICAL SUBDIVISION OF THE BOHEMIAN MASSIF ON THE TERRITORY OF THE CZECH REPUBLIC. Journal of the Czech Geological Society, 39/1, 127-144.

Chlupáč, I., (1993). Geology of the Barrandian. A Field Trip Guide. Senckenberg-Buch 69, Frankfurt, 163p.

Chlupáč, I., Brzobohatý, R., Kovanda, J., Stráník, Z., (2011). Geological history of the Czech Republic. Academia, Prague, in Czech, 436p.

Durand, G., Gagliardini, O., Thorsteinsston, T., Svensson, A., Kipfstuhl, J., Dahl-Jensen, D., (2006). Ice microstructure and fabric: an up to date approach to measure textures. J. Glaciol., 52 (179), 619–630.

Fürst, V., (2005). The pond Dolní Tušimy in the basin of right-hand tributary of Voznický stream. Report 2, 05-01/MŘDT-JCM, in Czech.

Gay, M., Wiess, J., (1999). Automatic reconstruction of polycrystalline ice microstructure from image analysis: application to the EPICA ice core at Dome Concordia, Antarctica. Journal of Glaciology, vol. 45, no. 151, pp. 547-554.

Gow, Anthony J., Langston, D., (1977). Growth history of lake ice in relation to its stratigraphic, crystalline and mechanical structure. CRREL Report 77-1, 24p.

Hem, John D., (1989). Study and Interpretation of the Chemical Characteristics of Natural Water. Third Edition, Alexandria, VA: Department of the Interior, U.S. Geological Survey, Water-Supply Paper 2254, 263p.

Heron, R., (1983). AIR BUBBLE STRATIGRAPHY OF LAKE ICE COVERS (Abstract only).

Hertl, A., Vikhamar, D., (1999). Ice core stratigraphy:comparision of glacier ice cores and lake ice cores in the Tarfala Valley. GLACIOLOGICAL FIELD COURSE TARFALA RESEARCH STATION / NORTHERN SWEDEN.

Hindman, B., (2006). What Is an iButton Device? APPLICATION NOTE 3808, Maxim integrated, http://www.maximintegrated.com/app-notes/index.mvp/id/3808 - 3.8. 2013.

Hinkel, Kenneth M., (1983). ICE-COVER GROWTH RATES AT NEARSHORE LOCATIONS IN THE GREAT LAKES. NOAA Technical Memorandum ERL GLERL-44, 35p.

Hrubá, J., Kletetschka, G., (2013). Thermal relations leading to the formation of gaseous phase within the ice covering lakes and ponds. AGU Fall Meeting, Abstract, Control #: 1814211.

Hubbart, J., Link, T., Campbell, C., Cobos, D., (2005). Evaluation of a low-cost temperature measurement system for environmental applications. *Hydrol. Process.* 19, 1517–1523.

Ibrahim, A. A., Balogun, A. A., Iguisi, E. O., Nduka, I. C., (2009). EVALUATION OF A LOW-COST TEMPERATURE MEASUREMENT SYSTEM FOR THE INVESTIGATION OF THE CHARACTERISTICS OF THE URBAN CANOPY HEAT ISLAND IN KANO CITY, NIGERIA. The seventh International Conference on Urban Climate, 29 June - 3 July 2009, Yokohama, Japan, 4p.

Inada, T., Hatakeyama, T., Takemura, F., (2009). Gas-storage ice grown from water containing microbubbles. International journal of refrigeration 32, 462-471.

Jeffries, Martin O., Morris, K., (2006). Instantaneous daytime conductive heat flow through snow on lake ice in Alaska. Hydrol. Process. 20, 803–815.

Keuschnig, M., Hartmeyer, I., Schmidjell, A., Schrott, L., (2012). The adaptation of iButtons® for near-surface rock temperature and thermal offset measurements in a high alpine environment – Instrumentation and first results, Kitzsteinhorn (3203 m), Hohe Tauern, Austria. Geophysical Research Abstracts, vol. 14, EGU 2012-12981.

Kletetschka, G., Fischer, T., Mls, J., Dědeček, P., (2013). Temperature fluctuations underneath the ice in Diamond Lake, Hennepin County, Minnesota. Water Resources Research, vol. 49, issue 6, 3306-3313.

Kottek, M., Grieser, J., Beck, C., Rudolf, B., Rubel, F., (2006). World Map of the Köppen-Geiger climate classification udaten. Meteorologische Zeitschrift, vol. 15, no. 3, 259-263.

Langway, C.C., (1958). Ice fabrics and the universal stage, Techn. Rep. 62. U.S. Army Snow, Ice, and Permafrost Research Establishment, Hanover, N.H.

Leppäranta, M., (1993). A Review of Analytical Models of Sea-Ice Growth. ATMOSPHERE-OCEAN 31 (1), 123-138.

Leppäranta, M., Kosloff, P., (2000). The Structure and Thickness of Lake Pääjärvi Ice. Geophysica, 36 (1-2), 233 – 248.

Liston, Glen E., Hall, Dorothy K., (1995). An energy-balance model of lake-ice evolution. Journal of Glaciology, vol. 41, no. 138, 373-382.

Livingstone, D. M., Adrian, R., Blencker, T. , George, G., Weyhenmeyer G. A. (2010). Lake ice phenology. In: George, D.G. (ed). The impact of climate change on European lakes. Aquatic Ecology Series 4:51–62.

Madrazo, C., Tsuchiya, T., Sawano, H., Koyanagi, K., (2009). Air Bubbles in Ice by Simulating Freezing Phenomenon. The Journal of the Society for Art and Science, vol. 8, no. 1, pp. 35-42.

Maeno, N., (1967). Air Bubble Formation in Ice Crystals. In Physics of Snow and Ice: proceedings, Hokkaido University Collection of Scholarly and Academic Papers : HUSCAP, pp. 207-218.

McCann, T., (2008). The Geology of Central Europe, Volume 1: Precambrian and Paleozoic. The Geological Society, London, 748p.

Mullen, Peter C., Warren, Stephen G., (1988). Theory of the Optical Properties of Lake Ice. Journal of Geophysical Research, vol. 93, no. D7, 8403-8414.

Müller-Stoffels, M., Langhorne, Pat J., Petrich, Ch., Kempema, Edward W., (2008). Preferred crystal orientation in fresh water ice. Cold Regions Science and Technology 56, 1-9.

Nikanorov, A. M., Brazhnikova, L. V., (2004). Water Chemical Composition Of Rivers, Lakes And Wetlands. In TYPES AND PROPERTIES OF WATER – Vol. II, Encyclopedia of Life Support System (EOLS).

Pitter, P., (1999). Hydrochemie. Vydavatelství VŠCHT, Prague, in Czech,568p.

Pretel, J., Bartoš, J., Bučilová, R., Chvojková, P., Černá, M., Fott, P., Grabmülerová, D., Kalvová, J., Kálal, J., Kašpárek, L., Kolda, M., Kubečka, J., Kužel, J., Lippert, E., Malý, M., (2001). ON THE UN FRAMEWORK CONVENTION ON CLIMATE CHANGE, THE CZECH REPUBLICiS THIRD NATIONAL COMMUNICATION. Ministry of the Environment of the Czech Republic Czech Hydrometeorological Institute, Prague, 130p.

Prowse, T. D**.**, Bonsal, B., Duguay, C. R., Hessen, D. O. and Vuglinsky, V. S., (2007). Chapter 8: River and Lake Ice. In: Global Outlook for Ice & Snow. United Nations Environment Programme, pp 201-213.

Rafferrty, John P., (2012). Glaciers, Sea Ice, and Ice Formation. Britannica Educational Publishing, New York, 255p.

Roessiger, J., Bons, Paul D., Faria, Sérgio H., (2012). Influence of bubbles on grain growth in ice. Journal of Structural Geology xxx, 1-10.

Scharlin, P., Battino, R., Silla, E., Tuñón, I., Pascual-Ahuir, J. L., (1998). Solubility of gases in water: Correlation between solubility and the number of water molecules in the first solvation shell. Pure &Appl. Chem., vol. 70, no. 10, pp. 1895-1904.

Shaw, B., Mechenich, C., Klessig, L., (2004). Understanding lake data. University of Wisconsin–Extension, Cooperative Extension, 20p.

Voženílek, V., Míková, T., Vakeriánová A., (2007). Atlas podnebí Česka/ Climate Atlas of Czechia. First Edition, Prague, 256p.

Wolaver, B. D., Sharp Jr., J. M., (2007). Thermochron iButton: Limitation of this Inexpensive and Small-Diameter Temperature Logger. Ground Water Monitoring & Remediation 27, no. 3, 127-128.

Wu, H. (Hung-Ta), Chung, Tsair-Wang (2011). Chapter 13: Effect of Surface Tension on Mass Transfer Devices. In: Mass Transfer in Multiphase Systems and its Applications, Prof. Mohamed El-Amin (Ed.), ISBN: InTech, pp 273-300.

Yoshimura, K., Inada, T., Koyama, S., (2008). Growth of Spherical and Cylindrical Oxygen Bubbles at an Ice-Water Interface. Crystal Growth & Design, vol. 8, no. 7, 2108-2115.

Zhekamukhov, M. K., (1976). Distribution of dissolved gas in water and bubbles in ice upon movement of a crystallization front. Journal of engineering physics, Volume 31, Issue 4, pp 1158-1162.

5.1 Internet references

http://jmis2.jsdi.cz/arwis/smis/archive_big.php - 23.3. 2012

http://www.blueiceonline.com/howsite/icecore_schema.html - 6.5. 2013

http://www.datasheets.maximintegrated.com/en/ds/DS1922L-DS1922T.pdf - 5.8. 2013

http://www.geology.cz/app/ciselniky/lokalizace/show_map.php?mapa=g50&y=759000&x=1073300&s=1 – 16.8. 2013

http://www.rsd.cz

6. APPENDIX

Appendix 1: Copyright permission

maxim integrated

AUTHORIZATION FOR LIMITED USE OF MAXIM MATERIAL
Copy and Use Restrictions

THE MATERIALS CONTAINED ON THE MAXIM INTERNET WEBSITE ARE PROTECTED BY COPYRIGHT LAWS, INTERNATIONAL COPYRIGHT TREATIES, AND OTHER INTELLECTUAL PROPERTY LAWS AND TREATIES. EXCEPT AS OTHERWISE STATED HEREIN, THESE MATERIALS MAY NOT BE REPRODUCED, MODIFIED, DISPLAYED OR DISTRIBUTED IN ANY FORM OR BY ANY MEANS WITHOUT THE PRIOR WRITTEN CONSENT OF MAXIM. USE OF ANY MAXIM TRADEMARKS MUST ATTRIBUTE OWNERSHIP TO MAXIM AS APPLICABLE.

Upon Maxim's receipt of a copy of this Authorization form signed by You, Maxim hereby grants You permission to download, reproduce, display and distribute the Materials posted on its site solely for informational and non-commercial or personal use subject to the following terms and conditions:

1. No modifications may be made to the Materials.
2. All copyright and proprietary notices as they appear in such Material shall remain in such Material.
3. The following credit line must appear in such Material: "Copyright MaximIntegrated Products (http://www.maximintegrated.com). Used by permission."
4. Any unauthorized reproduction, disclosure, distribution or use of any Maxim Application Notes, Reference Designs and other such Design Materials shall be reported promptly to Maxim.
5. Use of Maxim trademarks in literature must attribute ownership to Maxim by use of a footnote indicating the word, name, symbol or device and applicable ownership by Maxim.

MAXIM DOES NOT WARRANT OR MAKE ANY REPRESENTATIONS REGARDING YOUR USE OR REPRODUCTION OF THE MAXIM DATA SHEETS OR IN TERMS OF THEIR CORRECTNESS, ACCURACY, RELIABILITY, CURRENTNESS, OR OTHERWISE.

By signing this Authorization, You agree to the terms and conditions herein and agree to defend and indemnify Maxim, its officers, directors, employees and agents from any and all damages, liability or causes of action, whether known or unknown incurred in connection with any claim, lawsuit or action that arises or results from Your use or reproduction of any Maxim material.

Please complete the information below, sign where indicated, and return the original to:
Maxim Integrated Products, Inc.
Attn: MarCom
160 Rio Robles
San Jose, CA 95134
memcenter@maximintegrated.com

JOLANA HRUZA
Your Name (Printed)

Date: 16/8/2013

Signature

Telephone: 00420723830451 Email: JOLANAHRUZA12@GMAIL.COM

MOKROVATY 120, NOVY KNIN 262 03, CZECH REPUBLIC
Street Address, City & State and Zip Code

PART OF MASTER WORK - CHARLES UNIVERSITY IN PRAGUE
Brief Explanation of Use

TEMPERATURE LOGGER iBUTTON WITH 8KB DATA-LOG MEMORY, 19-4990; REV 10; 4/11
Description of Material (Web Address (URL), Data Sheet, Application Note, Photograph, Artwork, Mark, Intellectual Property, etc.)
WHAT IS AN iBUTTON DEVICE? APPLICATION NOTE 3808

Material Authorization, Vev. 04, 20130711.km Page 1 of 1

Gmail

Jolana Hruba <jolanahruba12@gmail.com>

SPR 221135 [Closed] - References

Počet zpráv: 2

support-center@support.maximintegrated.com <support-center@support.maximintegrated.com> 17. srpna 2013 3:24
Komu: jolanahruba12@gmail.com

| -- Any reply text must be above this line --
|==========
|
| SPR 221135 - Close Request - Maxim Support Center
|
| STATUS UPDATE.
| This request is now closed within our system. You may reply
| within the next 10 days if you feel this matter is not
| resolved. You can also reply by using our fast and secure
| webform here:
|
| https://support.maximintegrated.com/rtd/reply.mvp?id=221135&code=1F97CD1000
|
| QUALITY OF SERVICE REVIEW:
| If you would like to provide feedback regarding the service
| you received for this specific request, use the following
| webform within the next 10 days:
|
| https://support.maximintegrated.com/rtd/qos.mvp?id=221135&code=1F97CD1000
|
|==========
| Staff Comment 2013-08-15 20:24:30 PST
| By: Therese M
|
| Hi, Jolana:
|
| Thank you for returning these documents.
|
| You may now cite Maxim as agreed to within the document.
|
| Good luck with your Masters work!
|
| Best regards,
| Therese Montgomery
| System Applications Engineering
| Maxim Integrated
|
|----------